Characterization of the *Neisseria meningitidis* Helicase RecG

Getachew Tesfaye Beyene[1¤], Seetha V. Balasingham[2], Stephan A. Frye[2], Amine Namouchi[2], Håvard Homberset[1], Shewit Kalayou[1], Tahira Riaz[1], Tone Tønjum[1,2]*

1 Department of Microbiology, University of Oslo, Oslo, Norway, 2 Department of Microbiology, Oslo University Hospital (Rikshospitalet), Oslo, Norway

¤ Current address: College of Health Sciences, Mekelle University, Mekelle, Ethiopia
* tone.tonjum@medisin.uio.no

CrossMark
click for updates

Abstract

Neisseria meningitidis (Nm) is a Gram-negative oral commensal that opportunistically can cause septicaemia and/or meningitis. Here, we overexpressed, purified and characterized the Nm DNA repair/recombination helicase RecG (RecG$_{Nm}$) and examined its role during genotoxic stress. RecG$_{Nm}$ possessed ATP-dependent DNA binding and unwinding activities *in vitro* on a variety of DNA model substrates including a Holliday junction (HJ). Database searching of the Nm genomes identified 49 single nucleotide polymorphisms (SNPs) in the *recG*$_{Nm}$ including 37 non-synonymous SNPs (nsSNPs), and 7 of the nsSNPs were located in the codons for conserved active site residues of RecG$_{Nm}$. A transient reduction in transformation of DNA was observed in the Nm *ΔrecG* strain as compared to the wildtype. The gene encoding *recG*$_{Nm}$ also contained an unusually high number of the DNA uptake sequence (DUS) that facilitate transformation in neisserial species. The differentially abundant protein profiles of the Nm wildtype and *ΔrecG* strains suggest that expression of RecG$_{Nm}$ might be linked to expression of other proteins involved in DNA repair, recombination and replication, pilus biogenesis, glycan biosynthesis and ribosomal activity. This might explain the growth defect that was observed in the Nm *ΔrecG* null mutant.

Introduction

Neisseria meningitidis (Nm), or the meningococcus, is a Gram-negative bacterium that frequently colonizes the human oropharynx. In individuals who lack bactericidal antibodies, Nm can enter the bloodstream, cross the blood-brain barrier, and cause septicaemia and/or meningitis [1]. We are interested in how Nm cells survive on the oral mucosal surface, in the bloodstream and at the meninges, where it is exposed to reactive oxygen and nitrogen species that are typically highly genotoxic [2]. DNA repair pathways that promote genome stability and protect against oxidative DNA damage have been extensively characterized in *Escherichia coli*; however, the comparable DNA repair pathways in Nm are less well studied. It has been reported that *Neisseria* may be less proficient in DNA base excision repair (BER) than *E. coli* and also lacks an SOS response to DNA damage [2,3]. These features, and its genetic tractability due to its constitutive competence for transformation and short generation time, make Nm

an excellent organism for investigating DNA repair mechanisms and pathways in a host-adapted pathogen [4].

Helicases play major roles in genome maintenance including repair, recombination and replication of DNA in all kingdoms of life. Due to the complexity of the DNA damage responses, very little is known about how helicase-dependent DNA repair pathways are regulated and coordinated with cell cycle checkpoints [5]. RecG is ubiquitous among bacterial species [6, 7], vascular plants and green algae [7] where it is targeted to mitochondria and chloroplast [8], however, homologues of RecG have not been detected in other eukaryotes or archaea. Bacterial RecG has two RecA-like helicase domains, an N-terminal wedge-containing domain and a C-terminal TRG (<u>t</u>ranslocation by <u>RecG</u>) motif [9]. The RecG protein in *E. coli* (RecG$_{Ec}$), which is extensively studied by Lloyd and co-workers, inhibits inappropriate DNA replication and aberrant chromosome segregation in cells exposed to UV irradiation [10]. RecG is also essential in *E. coli* cells lacking 3′ single-stranded DNA exonucleases to counteract PriA helicase-mediated DNA re-replication [11]. Homologous recombination is a fundamental cellular process that rearranges genes within and between chromosomes, promotes DNA repair and guides segregation of chromosomes [12]. In bacteria, RecG and RuvAB play critical roles in processing HJs and promoting branch migration [13]. RecG-deficient bacterial cells exhibit complex and variable phenotypes, including defects in transformation and pilin antigenic variation in Nm [14,15], defective growth and reduced radio-resistance in *Deinococcus radiodurans* [16], sensitivity to oxidative stress in *Pseudomonas aeruginosa* [17], and sensitivity to UV radiation in *P. aeruginosa* and Nm [14,17].

In this study, RecG$_{Nm}$ was characterized and its roles in DNA recombination, repair, replication and transformation explored. Recombinant RecG$_{Nm}$ was assessed for its DNA binding and unwinding activities on model DNA substrates in the presence and absence of ATP. Nm wildtype and Δ*recG*$_{Nm}$ cells were compared with respect to cellular phenotype, response to genotoxic stress and protein expression signatures. The results provide insight into the possible biological roles of RecG$_{Nm}$.

Materials and Methods

Cloning of the *N. meningitidis recG* and *ssb* genes

The Nm *recG* and *ssb* genes were PCR amplified from genomic DNA isolated from Nm strain MC58 using the primers listed in S1 Table. In brief, the ORF encoding *recG*$_{Nm}$ in Nm strain MC58 was amplified by PCR using the primers GTB3 and GTB5 (S1 Table). The PCR product was cloned into the pET28b (+) plasmid (Novagen). The resulting plasmid, pGTB1, with an N-terminal 6xHis-tag, was transformed into *E.coli* ER2566. A construct pGTB1K294A bearing a point mutation in the ATP binding motif (K294A) was created from pGTB1 by site-directed mutagenesis using primers GTB17 and GTB18 (S1 Table). The Nm *ssb* gene cloning was performed as previously described [18]. For the construction of *ssb*NmΔC8 expressing a C-terminally truncated SSB$_{Nm}$ protein, primers SF275 and SF276 were used to amplify the vector pSAF104 using the vector pEH1 as a template (S1 Table). The PCR product was joined by Gibson assembly [19] and, transformed into *E. coli*. Constructs were verified by sequencing.

Overexpression, purification and characterization of recombinant proteins

The recombinant RecG$_{Nm}$ was overexpressed in *E. coli* and the RecG$_{Nm}$ protein was purified to homogeneity (S1 Fig). Briefly, the *E. coli* ER2566 cells harbouring plasmid pGTB1and pGTB1K294A were grown at 37°C in LB medium containing 50 µg/ml kanamycin until

$OD_{600nm} \approx 0.4$, the temperature was reduced to 18°C. Protein expression was induced with 0.5 mM isopropyl β-D-thiogalactopyranoside (IPTG) overnight. Cells were harvested by centrifugation and resuspended in lysis buffer, disrupted by sonication and the lysates were used as source material to purify $RecG_{Nm}$ by affinity chromatography on Ni-NTA followed by gel filtration on Superdex 75. The SSB_{Nm} and $SSB_{Nm\Delta C8}$ proteins were purified as previously described [18].

Model DNA substrate preparation and DNA binding, unwinding and ATPase assays

Preparation of DNA substrates. DNA oligonucleotides used in this study to generate model DNA substrates were adapted from previous studies [7,20–22]. DNA substrates were prepared essentially as described in [7]. Briefly, oligonucleotides were 5′-end labelled using γ-^{32}P[ATP] (PerkinElmer) and T4 PNK enzyme (NEB) for 1 h at 37°C. Unincorporated ATPs were removed using illustra Microspin™ G-25 columns (GE Healthcare). Labelled and unlabelled complementary oligonucleotides were mixed at a molar ratio of 1:2.5, in annealing buffer [40 mM Tris-HCl (pH 8.0), 50 mM NaCl] and denatured at 95°C for 5 min and allowed to cool down to room temperature overnight. The annealed products were resolved on 8% non-denaturing polyacrylamide gel. The bands containing the completely annealed substrates were excised and DNA was eluted into [10 mM Tris-HCl (pH 8.0), 0.5 mM EDTA] buffer overnight at 4°C. The concentrations of the eluted DNA substrates were estimated as described elsewhere in [23]. For the ATPase assay, branched DNA substrates were prepared as indicated above except that the complementary oligonucleotides were not labelled with γ-32P[ATP] and the annealed products were not gel purified as previously described in [24]. The schematic diagram of the DNA substrates and DNA sequences are presented in Fig 1 and S2 Table, respectively.

Band shift assay. Band shift assay was carried out as described in [7]. Reaction mixtures (20μl) contained 0.1 nM γ-^{32}P-labelled DNA substrates, binding buffer [40 mM Tris-HCl, (pH 8), 2.5 mM EDTA, 2 mM MgCl2, 100 mg/ml bovine serum albumin (BSA), 6% glycerol, and 1 mM DTT] and the indicated concentrations of the $RecG_{Nm}$ or $RecG_{Nm}K294A$ protein. After incubation for 15 min on ice, 2 μl of 60% glycerol was added to the reaction immediately before loading on to a 30 min pre-run 5% native PAGE gel (29:1, acrylamide: bisacrylamide). Electrophoresis was done using low ionic strength buffer (6.7 mM Tris HCl pH 8, 3.3 mM sodium-acetate pH 5.5 and 2 mM EDTA pH 8) at 200V for 5 min followed by 160 V for 85 min in ice water bath with continuous buffer recirculation between the upper and lower chambers. Gels were dried using GD 2000 Vacuum Gel Dryer (Hoefer®, Inc). The products were visualized using Typhoon PhosphorImager, and the gel bands were quantitated using ImageQuant TL v2003.02 (GE Healthcare). Percent DNA bound was calculated as follows: percent DNA bound = (B/ (B+F)) x 100, where B is the bound DNA and F is the free DNA.

Helicase assays. All helicase unwinding reactions (10μl) were carried out in helicase reaction buffer [20 mM Tris-HCl (pH 7.5), 50 mM NaCl, 1 mM DTT, 2 mM MgCl$_2$, 2 mM ATP and 50 mg/ml BSA]. 0.1 nM γ-^{32}P-labeled DNA substrate was mixed with increasing concentration of $RecG_{Nm}$ or $RecG_{Nm}K294A$ and incubated at 37°C for 30 min. The reaction was terminated by adding 5μl of 3x stop dye (50 mM EDTA, 40% glycerol, 0.9% SDS, 0.1% bromophenol blue and 0.1% xylene cyanol) along with 10x molar excess unlabeled oligonucleotide complementary to the unlabeled strand in the substrate. The reaction products were analyzed on 8% native polyacrylamide (19:1) gel containing 0.1% SDS in 1x Tris/borate/EDTA buffer. Gels were dried, exposed, visualized and quantitated as described for DNA binding assay. Percent helicase unwound was calculated as follows: percent unwound = (P/(S+P)) x 100, where P is the product and S is the residual substrate. Values of P and S were determined
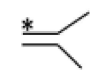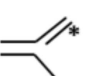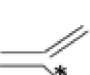
number	name	structure	oligonucleotide composition	binding activity	unwinding activity
1	forked DNA duplex		5*+6	+	-
2	lagging strand replication fork		5+6+7*	+	+
3	leading strand replication fork		5+6+8*	+	+
4	complete replication fork		5+6+7*+8	+	+
5	Holliday junction		1*+2+3+4	+	+
6	bubble		9*+10	+	-
7	5′-hairpin-tailed D-loop		9+10+13*	+	+
8	5′-tailed D-loop		9+10+11*	+	+
9	3′- tailed D-loop		9+10+12*	+	+

Fig 1. Schematic diagram of model DNA substrates, and the RecG$_{Nm}$ DNA binding and unwinding activity. Minus and plus symbols indicate the absence or presence of RecG$_{Nm}$ activity on the indicated substrate, respectively.

by subtracting background values in controls having no enzyme and heat denatured substrate, respectively. The Kd value of the data obtained from binding and unwinding assay was analysed using GraphPad Prism 5 with curve fitting using nonlinear regression.

ATPase assay. RecG$_{Nm}$ ATP hydrolysis activity was monitored by thin-layer chromatography (TLC), as previously described [7]. RecG$_{Nm}$ or RecG$_{Nm}$K294A was added to initiate a 10 μl reaction in the presence of 100nM DNA cofactor in ATPase buffer [20 mM Tris/HCl (pH 7.5), 2 mM MgCl$_2$, 100 μg BSA/ml, 25 mM cold ATP, 0.023 nM [γ-^{32}P]ATP, 2 mM DTT]. Also reactions containing DNA cofactor but without the wild type (RecG$_{Nm}$) protein, and RecG$_{Nm}$ but without DNA cofactor were included per experiment. The reaction mixture was incubated at 37°C for the indicated times and terminated by adding 5 μl of 0.5 M EDTA (pH 8.0). Samples (2 μl) were spotted onto TLC plates (PEI Cellulose F, Merck) at 1.5 cm intervals and resolved using a solution containing 1 M formic acid and 0.5 M LiCl. The TLC plates were

air-dried, exposed to a phosphorimaging screen, imaged and quantified as described above for the DNA binding assays. The percentage of hydrolyzed ATP was calculated as {counts for γ-32Pi / (counts for γ-32Pi+counts for [γ-32P]ATP)} x 100. The values obtained from samples lacking RecG$_{Nm}$ were subtracted from the samples containing RecG$_{Nm}$ to account for background ATP hydrolysis.

Construction of an *N. meningitidis ΔrecG* mutant

The *recG* DNA fragments were designed to recombine and integrate into the host chromosome allowing the *recG* gene to be interrupted by an antibiotic resistance gene. For this purpose, primer pairs SF81/SF82 and SF83/SF84 were used to amplify two regions covering bp 343–821 and bp 893–1439 of the *recG* gene, respectively. These were then ligated with a kanamycin resistance gene (*aph*) and the pBluescriptIISK+ vector (Stratagene) by 4-point ligation. The resulting plasmid, pSAF48, conferring resistance to ampicillin and kanamycin, was transformed into XL1-Blue (Stratagene) for plasmid propagation. The sequence of the insertion was verified by DNA sequencing. The plasmid was transformed into Nm strains MC58, M1080 and M400 and *Neisseria gonorrhoeae* (Ng) strains MS11 by natural transformation using kanamycin resistance as selective marker for null mutants.

Bacterial strains and growth conditions

The bacterial strains and plasmids employed in this study are listed in Table 1. Neisserial strains were grown on GC agar plates or in liquid GC medium (7.5 g/l peptone, 3.75 g/l tryptone, 4 g/l K$_2$HPO$_4$, 1 g/l KH$_2$PO$_4$, 5 g/l NaCl) supplemented with IsoVitaleX at 37°C and 5% CO$_2$. When required, kanamycin at a final concentration of 100 mg/l was added. *E. coli* was grown in LB medium or on LB plates containing kanamycin (50 mg/l) at 37°C. Nm wildtype and Nm *ΔrecG* mutant strains were grown at 34°C in 5% CO$_2$ for 18–24 hours. Growth properties were assessed by comparing colony edges (sharp or diffuse) [25], colony size and colony number on GC plates with 1% agar. Pictures of meningococcal colonies were taken using a stereo microscope (Leica) equipped with a CCD camera.

For colony size measurement, overnight grown Nm wildtype and Nm *ΔrecG* mutant cells were suspended in liquid GC medium and adjusted to OD$_{660}$ = 0.2. A tenfold serial dilutions of the cells were prepared in 1x PBS and 50 µl aliquots of the 10^{-6} dilutions were spread on GC agar plates. The plates were incubated with 5% CO$_2$ at 37°C for 18 hours. Pictures of whole plates were captured using a Lifecam camera (Microsoft) at a resolution of 8 megapixels. Colony count and colony size measurements were performed using the OpenCFU 3.8 BETA software [26] with settings for the minimum radius set to 2 pixels and the maximum radius set to Auto-Max.

Quantitative transformation assay

Quantitative transformation was performed as previously described [14,31] using plasmid pDV-c-d1 carrying an antibiotic resistance marker. Briefly, Nm cells were pre-grown on GC plates overnight at 37°C and resuspended in 5% CO$_2$ saturated GC medium containing IsoVitaleX and 7 mM MgCl$_2$. 5 µl of DNA (100 ng/µl) were provided in 15 ml tubes, 500 µl cell suspension was added, mixed and incubated at 37°C for 15 min without agitation followed by the addition of 25 U/ml benzonase and incubated at 37°C for 10 min to degrade extracellular DNA. Samples were diluted by adding 4.5 ml GC medium and incubated for 4.5 h at 37°C on a rotator drum at 60 rpm. Of each undiluted sample, 50 µl aliquots were spread on GC agar plates containing 8 mg/l erythromycin and 100 µl of 10^{-5} and 10^{-6} dilutions, prepared in PBS, were spread on GC agar plates without antibiotics. Following overnight incubation at 5% CO$_2$

Table 1. Bacterial strains and plasmid constructs employed in this study.

	Relevant characteristic	Source
Plasmids		
pET28b(+)	bacterial expression vector with T7 promoter; kanamycin resistance	Novagen
pGTB1	pET28b(+) based vector with $recG_{Nm}$ insert between *Xho*I and *Nde*I	This study
pGTB1K294A	pGTB1 based vector with site directed mutant of $recG_{Nm}$ in motif I	This study
pDV-c-d1	pBluescriptIISK+ based vector with *pilG*::*Erm*[r] and DUS	[27]
pEH1	pQE-30 harboring *ssb* from Nm MC58	[18]
pSAF104	pEH1-based plasmid harboring *ssb*NmΔC8	This study
Strains		
Escherichia coli		
ER2566	*fhuA2 lacZ*::T7 gene1 [lon] ompT gal *sulA11* R(mcr-73::miniTn10—Tet[S]) 2 [dcm] R(zgb-210::Tn10—Tet[S]) *endA1* Δ(*mcrC*-mrr)114::IS10.	New England Biolabs
XL-1 Blue	*recA1 endA1 gyrA96 thi-1 hsdR17 supE44 relA1 lac* [F′ *proAB lacI*q*Z*Δ*M15* Tn*10* (TetR)]	Stratagene
Neisseria meningitidis		
MC58	serogroup B, isolated in England	[28]
MC58Δ*recG*	derivative of MC58 with *recG*::*Kan*[r]	This study
M1080	serogroup B, isolated in the United States in 1984	[29]
M1080Δ*recG*	derivative of M1080 with *recG*::*aph*; kanamycin resistance	This study
M400	derivative of M1080 containing the IPTG -inducible *recA6* allele (TetM)	[30]
Neisseria gonorrhoeae		
MS11		Herman Schneider
MS11Δ*recG*	Derivative of MS11 with *recG*::*aph;* kanamycin resistance	This study

doi:10.1371/journal.pone.0164588.t001

and 37°C colonies were counted. Transformation frequency was calculated as the number of antibiotic-resistant colony forming units (CFU) per total CFU.

Spontaneous mutation assay

Spontaneous mutation rates were determined as previously described [4,32] with minor modifications. Briefly, overnight grown Nm wildtype and $\Delta recG_{Nm}$ cells were suspended in GC medium with the OD_{660} adjusted to 0.02. The suspension was further diluted 10 fold and the cells were grown at 37°C for 6 hours. Then, 50 μl of the undiluted and 10^{-1} diluted cells were spread on GC plates containing 3 mg/l rifampicin, whereas 10^{-5}, 10^{-6}, and 10^{-7} dilutions were spread on plain GC plates. The cells were grown for 24 hours at 37°C and 5% CO_2 and the colonies were counted. The mutation rate was calculated as a ratio of rifampicin-resistant colony forming unit (CFU) to the total number of CFU. The assay was repeated 5 times for each strain.

SDS-PAGE and immunoblotting

Procedures for sample preparation, SDS-PAGE and antigen detection have been described previously [33,34]. The presence of RecG, SSB and pilin, respectively, in Nm whole-cell lysates was detected by immunoblotting using rabbit polyclonal antiserum raised against recombinant $RecG_{Nm}$ and SSB_{Nm} and purified Nm pili.

Flow cytometry analysis

Nm can cause serious systemic infections [35], therefore, the relatively less invasive pathogen Ng was used to perform flow cytometry analysis outside the neisseria (biosafety level-2)

laboratory. Colonies of Ng MS11 wildtype and Ng $\Delta recG$ grown for 20–24 hours were suspended in CO_2-saturated liquid GC medium supplemented with IsoVitaleX to $OD_{660} \approx 0.02$. The cell suspension was diluted 10 times with GC medium and cells grown at 37°C overnight at 30 rpm to $OD_{660} \approx 0.16$. The cultures were further diluted 10 times and cells grown at 37°C for 4 doubling times at 60 rpm until $OD_{660} = 0.14$–0.18. Ng has a doubling time of 60 min at 37°C [36]. A 1 ml sample from the exponentially growing cultures of non-treated cells was collected and kept on ice until further processing. To 3 ml exponentially growing Ng cells, rifampicin (36 µg/ml) [37] and cephalexin (4 µg/ml) [38] were added, and cells were allowed to grow for additional six doubling times. Rifampicin inhibits initiation of replication but allows the current round of replication to continue to completion (replication runout), resulting in fully replicated chromosomes. Cephalexin stops cell division, resulting in integer numbers of chromosomes per cell [36,39]. Both, treated cells and non-treated control cells, were further processed as described elsewhere [40,41]. Briefly, the cells were pelleted at 14000×g for 4 min at 4°C, washed in TE buffer, resuspended in 100 µl TE buffer and fixed by addition of 900 µl 77% ethanol and incubated overnight. The fixed cells were washed in 1 ml ice cold 0.1M phosphate buffer (PB) and resuspended in 500 µl PB. The cells were stained with 1.5 µg/ml fluorescein isothiocyanate (FITC) in PB at 4°C overnight, washed in 1 ml ice-cold 0.02 M Tris-buffered saline (TBS; 20 mM Tris-HCl pH 7.5, 130 mM NaCl, pH 7.5). The cells were resuspended in 500 µl TBS with 1.5 µg/ ml Hoechst 33258 and kept for 30 minutes. Stained cells were passed through a 5 µm syringe Filter (Pall Life Sciences). To investigate the DNA content and chromosomal DNA replication patterns, slowly growing *E. coli* CM735, the majority containing one or two copies of chromosomal DNA [40], were used as standard to calibrate the flow cytometer. Sample processing was carried out as previously described [40] on a BD LSR II flow cytometer (BD Biosciences), and the data obtained from the flow cytometer were analysed using FlowJo version 10 software.

Genotoxic stress assays

Nm cells from overnight plate culture were suspended in liquid GC medium to $OD_{660} = 0.3$ and diluted 10 fold in CO_2 saturated GC medium containing IsoVitalex. The cells were allowed to grow for two hours at 37°C with rotation. 990 µl of the cells suspension was mixed with 10µl of 10 mM hydrogen peroxide, 50 mM paraquat, 1M MMS or 1µg/ml MMC. After the cells were grown for one additional hour with rotation at 37°C, 50 µl aliquots of 10^{-5} and 10^{-6} dilutions in PBS were spread on GC agar plates. To test sensitivity to ultraviolet radiation, 50 µl aliquots of 10^{-5} and 10^{-6} dilutions of non-treated cells were spread on GC agar plates, irradiated at UV intensities of 0–80 J/m^2 by using a CL-1000 Ultraviolet cross linker (Upland America). Finally, the plates were incubated overnight at 37°C with 5% CO_2 for 12 to 18 hours. Colonies were counted and survival rate was calculated as the ratio of the number of colony forming units (CFU) from treated to non-treated samples.

Bioinformatics analysis

Sequence data for alignment of the *recG* gene from *Neisseria* members was obtained from NCBI [42]. The Nm *recG* nucleotide sequences were searched for occurrences of the DNA uptake sequence (DUS) and single nucleotide polymorphisms, and the deduced RecG$_{Nm}$ amino acid sequence was searched for predicted structural motifs. The orientation of DUS was determined using The Sequence Manipulation Suite [43]. SNP analysis of the *recG* gene among 14 Nm strains available at Genbank was conducted using MEGA6 [44]. In the SNP analysis, only the first and the second codon positions were considered.

For the RecG 3D homology model, the sequence conservation was calculated from all available variants of NEIS0433 using plotcon from the EMBOSS package [45]. The variability was

visualized colour coded on the protein structure using ConSurf [46]. The Phyre2 service [47] was used to predict the 3D structure of the protein.

Proteomic analyses

i) Sample pre-treatment: Nm wildtype and *ΔrecG* cells of strain MC58 were harvested from GC agar plates. The cells were washed three times in PBS, inactivated at 60°C for 30 min, and resuspended in 2% SDS/10mM Tris-HCl, pH7.5 containing EDTA free protease inhibitor cocktail (Roche) and PhosStop (Roche). The samples were transferred to Lysing Matrix B tubes (Roche) and disrupted in a MagNa Lyser (Roche). The supernatant was collected and the protein concentration measured by Direct Detect (Millipore). Per sample 100μg of protein lysate was separated on 4–12% Bis-Tris polyacrylamide gel (Life technologies). Each gel lane was separated and divided into 6 pieces and the samples reduced with DTT (Sigma-Aldrich) followed by alkylation with iodoacetamide (Sigma-Aldrich) and in-gel digest with trypsin (Promega). The peptides were extracted from the gel pieces with acetonitrile and purified on C_{18} ZipTip prior to nLC-MS/MS analysis. ii) Mass spectrometry. Samples were injected into an EASY 1000 nLC (Thermo Scientific) coupled to a Q-Exactive MS (Thermo Scientific) using a data-dependent Top10 method. A two-column set up was used with pre-column (Acclaim PepMap 100, 75μm × 2cm, nanoviper, C18, 3μm, 100Å, Thermo Scientific) and analytical column (Pep-Map RSLC, C18, 2μm, 100Å, 50μm × 15cm, Thermo Scientific). Each sample was injected in triplicates. Peptides were separated using a 120 minutes gradient with solvent A (0.1% FA/3% ACN (FA:LC-MS grade, Fluka; ACN: LC-MS grade, Merck) and solvent B (0.1%FA/97% ACN) using the following steps: I) 2% to 30% B from start to 90 min, II) 30% to 45% B from 90 min to 100 min, III) 45% to 90% B from 100 min to 115 min, IV) 90% B from 100 min to 120 min. iii) Database search and statistics: MS results were analysed using MaxQuant software version 2 against the proteome from Nm MC58 (UP000000425, Uniprot). T-test calculations were performed in Perseus version 1.2.0.17 using the label free quantitative (LFQ) values. Differentially expression with a p-value <0.05 was considered to be statistically significant.

All functional categories were obtained using the Kyoto Encyclopedia of Genes and Genomes (KEGG) using blastKOALA [48]. Briefly, an in-house python script was used to retrieve and blast the sequences of the identified proteins using blastKOALA. Proteins with existing KEGG pathway, module, or functional hierarchy (BRITE) annotations were identified. In addition, we used the Cluster of Orthologous Classification (COG) from the NCBI database for functional protein group annotations.

Co-gel filtration interaction assay

The interaction between $RecG_{Nm}$, and SSB_{Nm}, and between $RecG_{Nm}$ and $SSB_{NmΔC8}$ was studied by gel filtration on a Superdex 200 10/300 GL column (GE Healthcare). Purified $RecG_{Nm}$ protein was mixed independently with SSB_{Nm} and with $SSB_{NmΔC8}$ proteins in a buffer consisting of 20 mM Tris pH (7.5), 600mM NaCl, and 1 mM DTT to a final volume of 300 μl. The samples were injected into a column equilibrated with the same buffer. The proteins were eluted in aliquots of 0.5 ml using the same buffer at 0.5 ml/min, and 13μl of each fraction was separated on SDS-PAGE and stained with Coomassie blue. The concentration of proteins used in the co-filtration assay was determined by DirectDetect (Millipore).

Microscale thermophoresis

Microscale thermophoresis (MST), a method for measuring molecule interaction, is described extensively elsewhere [49]. Labelling of SSB_{Nm} was carried out following the manufacturers' instructions using the Monolith NT Protein Labeling Kit RED–NHS (NanoTemper Technologies

GmbH) resulting in a degree of labelling (DOL) of 0.65. Different concentrations of RecG$_{Nm}$ were incubated with 21 nM SSB$_{Nm}$ in 20 mM HEPES buffer (pH 7.5) containing 300 mM NaCl, 0.05% Tween 20, 0.1% Pluronic F-127, 0.1% PEG 8000 and 2 mM DTT. Samples were immediately loaded into Premium Coated capillaries (NanoTemper Technologies GmbH) and measured at 22°C and 40% MST power.

Results

RecG$_{Nm}$ binds and unwinds DNA

The DNA binding ability of RecG$_{Nm}$ was investigated and using a band shift assay and DNA oligonucleotide substrates that resemble intermediates of DNA replication, repair and recombination. The experiments were performed with recombinant RecG$_{Nm}$ and ATPase-deficient RecG$_{Nm}$K294A. Both proteins showed equal ability to bind branched DNA substrates (Fig 2A and S1 Fig) and the HJ was the preferred substrate for binding (Fig 2B and S2 Fig). RecG$_{Nm}$ and RecG$_{Nm}$K294A also bind D-loop substrates containing a 5′-tail, 3′- tail or a hairpin-terminated tail (S3 Fig).

To test the specific unwinding activity on branched DNA substrates, increasing concentrations of RecG$_{Nm}$ were incubated with end-labelled DNA substrates in the presence of 2 mM ATP and Mg^{2+}. RecG$_{Nm}$ promoted branch migration of a HJ substrate generating flayed duplexes (Fig 3A) and unwound both strands of a complete replication fork (Fig 3B). The unwinding activity of RecG$_{Nm}$ was weaker on a leading strand replication fork than on a lagging strand replication fork (Fig 3C and 3D). RecG$_{Nm}$ also unwound a D-loop with a 5′- tail, 3′-tail or a hairpin-tail (S4 Fig). RecG$_{Nm}$K294A had no significant unwinding activity on any DNA substrate examined here (Fig 3).

RecG$_{Nm}$ is a DNA-dependent ATPase

The ATP hydrolysing activity of recombinant RecG$_{Nm}$ and RecG$_{Nm}$K294A was investigated using branched DNA cofactors such as forked DNA duplex, leading strand replication fork, lagging strand replication fork, and HJ; including circular ssDNA, circular dsDNA, and homopolymeric oligonucleotides. RecG$_{Nm}$ displayed comparable capacity of ATP hydrolysis in the presence of different types of branched DNA cofactors (Fig 1), as measured by the percentage of inorganic phosphate ($\approx$ 77%) released by the cleavage of the γ-phosphate. The efficiency with which RecG$_{Nm}$ hydrolysed ATP ($\approx$ 67% of input ATP) in the presence of circular ss- or ds- DNA was marginally less than its ATPase activity with branched DNA cofactors, yet not statistically significant (Fig 4); whereas RecG$_{Nm}$K294A nearly lost ATPase activity that is, $<$ 8% of the input ATP hydrolysed in the presence of branched DNA, circular ssDNA and circular dsDNA cofactors (Fig 4 and S5A Fig). RecG$_{Nm}$ also hydrolyzed ATP efficiently in the presence of homopolymeric ssDNA and dsDNA (S5B and S5C Fig), but RecG$_{Nm}$K294A had very weak ATP hydrolysis activity in the presence of these DNA cofactors. The ATPase activity of RecG$_{Nm}$ without DNA cofactor was almost non-detectable confirming that RecG$_{Nm}$ is a DNA-dependent ATPase (Fig 4 and S5 Fig).

Effect of Δ*recG$_{Nm}$* on colony morphology and colony size

Immunoblot analysis with an antibody against RecG confirmed that the resulting Nm Δ*recG* strains lack the RecG protein (Fig 5A). The absence of RecG in the Nm Δ*recG* mutant was also confirmed by mass spectrometry. Growth on solid media was compared for the parental Nm strains MC58 and M1080 and the respective *ΔrecG* derivative strains. Nm MC58Δ*recG* and M1080Δ*recG* produced more small-sized colonies than the corresponding wildtype strains (Fig
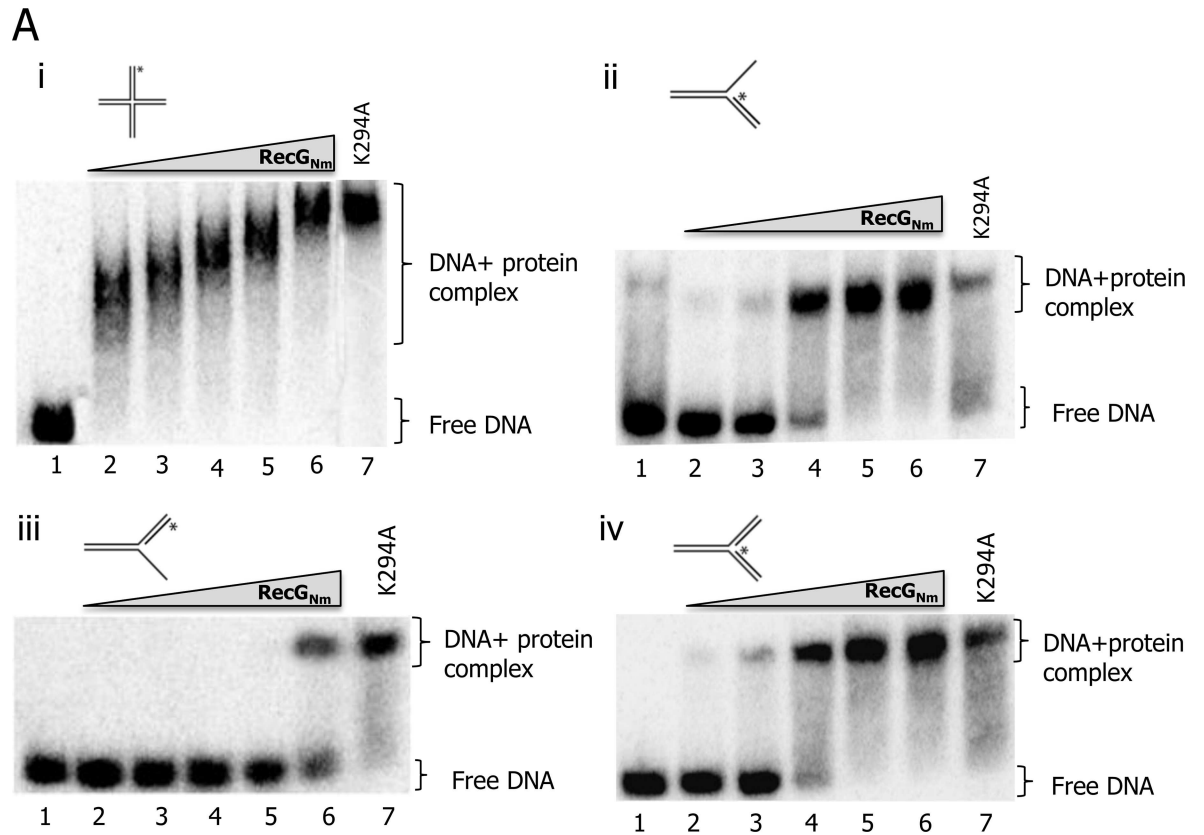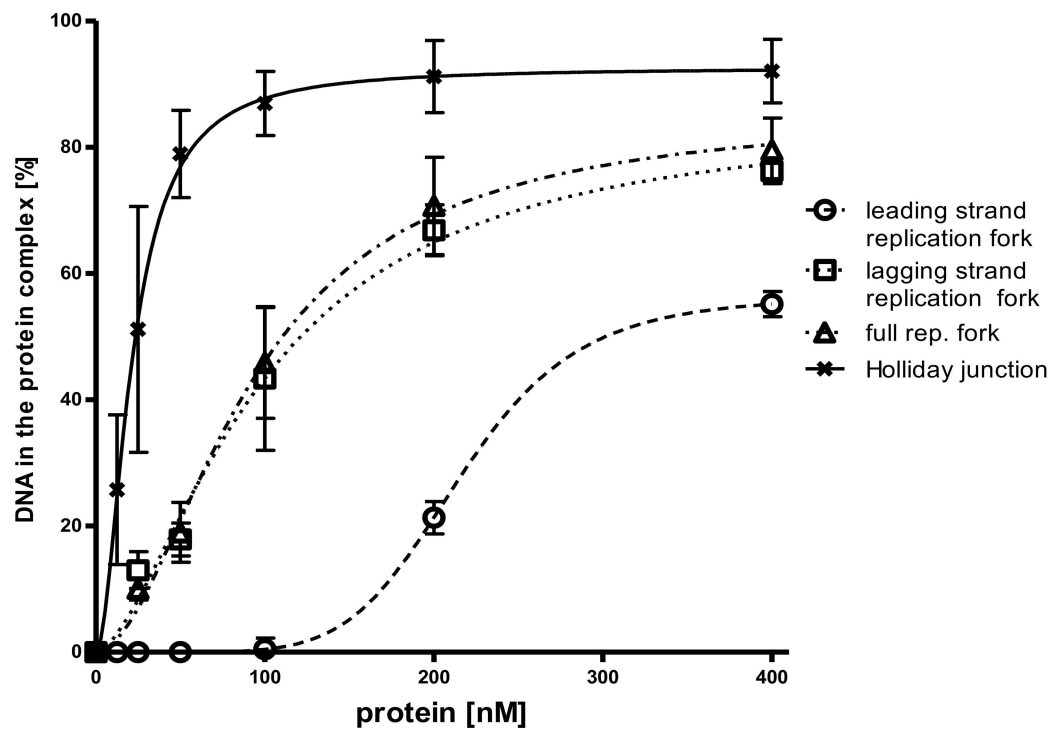
Fig 2. RecG$_{Nm}$ binds different model DNA substrates. A. Representative gel images of DNA binding assays where increasing amounts of RecG$_{Nm}$ was incubated with **i**. Holliday junction, ii. lagging strand replication fork, iii. leading strand replication fork, and iv). full replication fork. Lanes 1) reaction without protein; 2–6) 25, 50, 100, 200 and 400nM RecG$_{Nm}$, respectively, 7) 400nM RecG$_{Nm}$K294A. B. Quantitation of the gel images i, ii, iii, and iv in (A.) and the calculated Kd value for each Kd = 21.42, Kd = 97.79, Kd = 216.6, and Kd = 92.18, respectively. Data presented is mean ± SD from 3 independent experiments.

doi:10.1371/journal.pone.0164588.g002

5B). Large wildtype colonies were auto-agglutinating, while the small Δ*recG* colonies were not auto-agglutinating (Fig 5B). The average colony size was 6.8 (SD = 4.8) vs. 7.1 (SD = 6.9) mm^2 for MC58 mutant vs. wildtype and for M1080 8.6 (SD = 7.4) mm^2 and 4.5 (SD = 3.1) mm^2 for MC1080 mutant vs. wildtype (Fig 5C). The proportion of colonies 0 to 3.2 mm^2 was 19% for Nm MC58 wildtype and 3% for MC58 Δ*recG* and 27% and 38% for the M1080 wildtype and M1080 Δ*recG*, respectively.

As previously reported for Ng [14], Nm strain MC58 Δ*recG* demonstrated reduced competence for transformation. The reduced competence was only transiently observed, just after DNA was added (Fig 6 and S6 Fig). No significant change in spontaneous mutation rate was
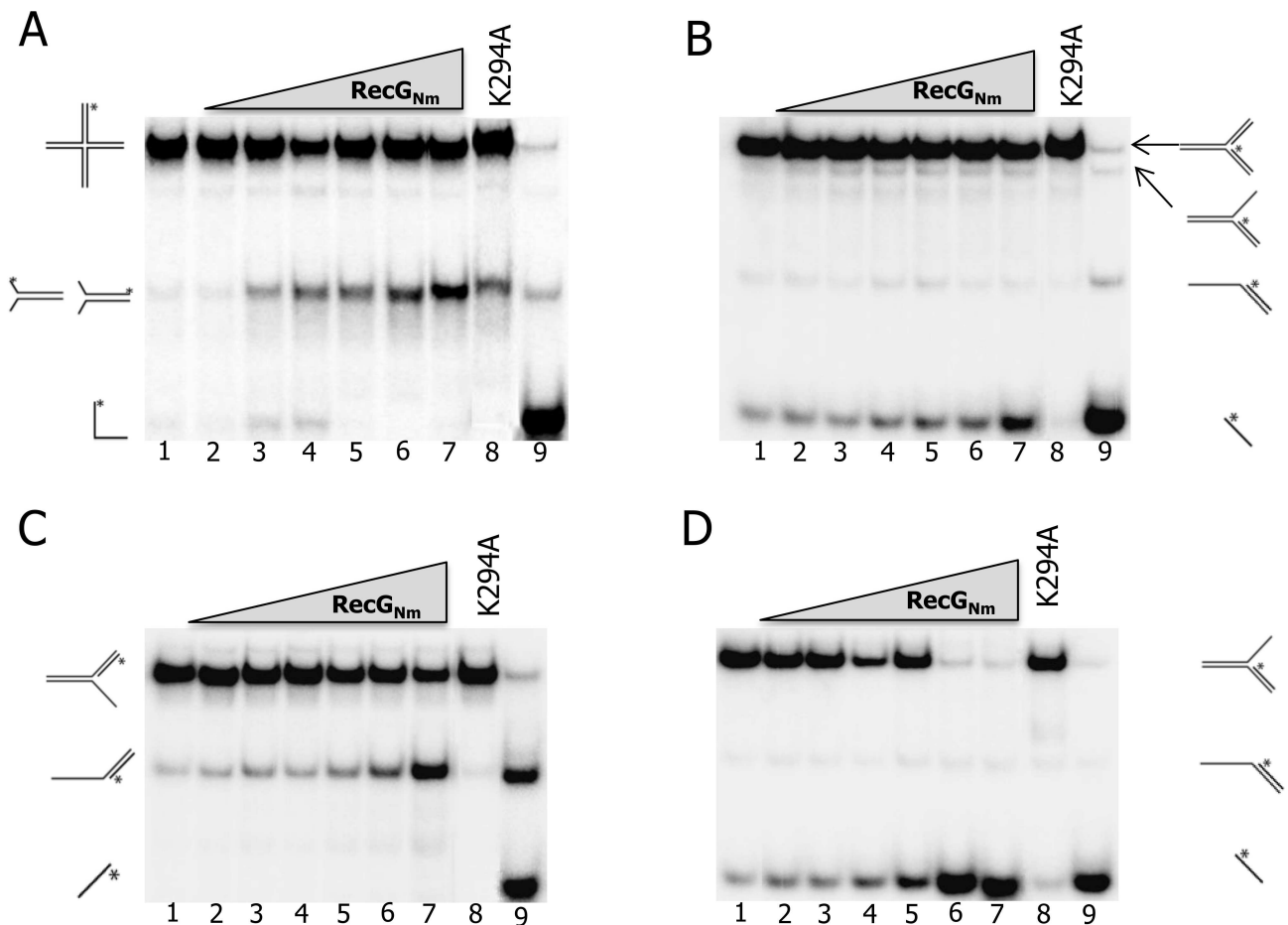

Fig 3. RecG$_{Nm}$ branch-migrates Holliday junction and catalyses unwinding of replication forks. Gel images of DNA unwinding assays where increasing amounts of RecG$_{Nm}$ was incubated with 0.1 nM A. Holliday junction, B. full replication fork, C. leading strand replication fork, D. lagging strand replication fork. Lanes: 1) reaction without enzyme, for Holliday junction substrate, 2–7) 12.5, 25, 50, 100, 200, and 400 nM RecG$_{Nm}$, respectively, 8) 400 nM RecG$_{Nm}$K294A; for fork substrates, 2–7) 1, 2, 4, 6, 12, and 25 nM RecG$_{Nm}$, respectively, 8) 25 nM RecG$_{Nm}$K294A, 9) Boiled substrate.
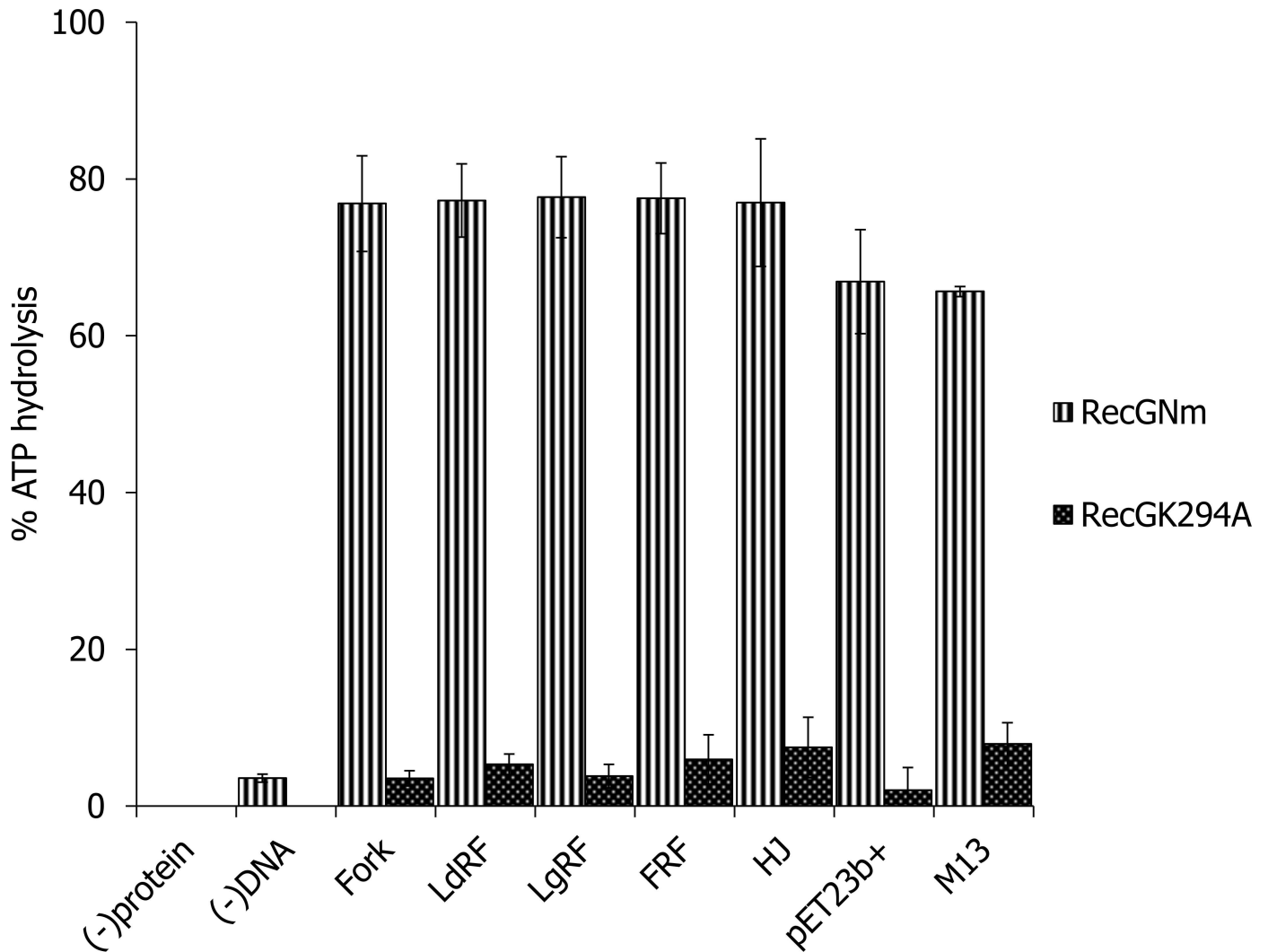
doi:10.1371/journal.pone.0164588.g003

Fig 4. RecG$_{Nm}$ is a DNA dependent ATPase. A graph showing ATPase activity of RecG from *Neisseria meningitidis* (RecG$_{Nm}$) and RecG$_{Nm}$K294A in the presence of DNA cofactors; forked DNA duplex, leading strand replication fork, lagging strand replication fork, HJ, M13mp18 ssDNA, and pET28b(+) dsDNA. % ATP hydrolysis is a measure of the percentage of inorganic phosphate released by the cleavage of the γ-phosphate of ATP. The standard deviations indicated by bars are from 3 independent experiments.

doi:10.1371/journal.pone.0164588.g004

observed in Nm Δ*recG* mutant strains. Spontaneous mutation rates of 2.4×10^{-8} (SD = 4.7×10^{-8}) and 2.3×10^{-8} (SD = 4.7×10^{-8}) were detected in Nm wildtype and Δ*recG*, respectively.

DNA replication and the number of replication forks

To estimate rate of cell growth and rate of DNA replication fork progression, total DNA content and total protein mass of Ng MS11 wildtype and Δ*recG* cells were measured. DNA content was measured from fluorescence intensity after staining with Hoechst 33258 and protein mass was estimated by performing flow cytometry on FITC-stained cells. The Ng MS11 wildtype and Δ*recG$_{Ng}$* mutant cells were used to estimate chromosome equivalents and the number of active replication forks per cell. For exponentially growing MS11 wildtype and Δ*recG$_{Ng}$*, DNA content was 276 and 251 (fluorescent in a̲r̲bitrary u̲nits, au), respectively. After treatment with rifampicin and CPX, DNA content was 277 and 262 au, respectively (S3 Table). Equal number of chromosome equivalents exists in MS11 wildtype and Δ*recG* mutant cells treated with
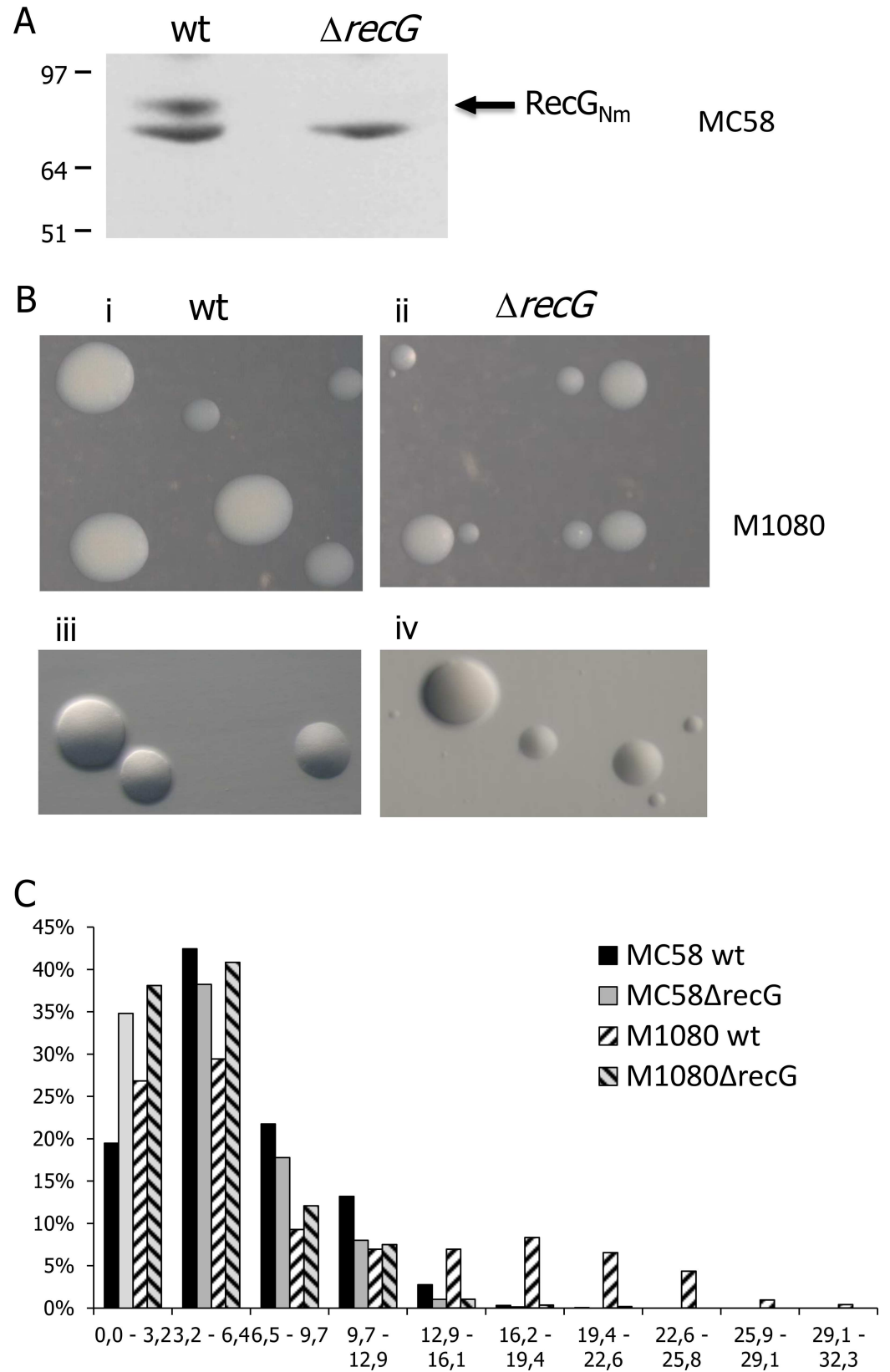
Fig 5. Phenotypic characterization of the NmΔ*recG* mutant. A. Immunoblot of cell lysates from *Neisseria meningitidis* (Nm) Mc58 wildtype and a Mc58Δ*recG* mutant detected with anti-RecG antiserum. B. Colony morphology of M1080 wildtype and M1080Δ*recG* null mutant of grown overnight at 34˚C, showing normal size colonies for the wildtype (i and iii), whereas the mutant strain shows normal size colonies together with small size colonies (ii and iv). C. Graphical presentation of the colony size measurement (area in mm^2) of the Nm wildtype strains and NmΔ*recG* Mc58 and M1080 mutant strains.

doi:10.1371/journal.pone.0164588.g005

rifampicin and CPX (Fig 7 and S7 Fig). This suggests no difference in the number of active replication forks in wildtype and mutant strains.

On the other hand, a slight difference was seen regarding the distribution of chromosome equivalents. For MS11Δ*recG*, 69% of the untreated and 64% of the treated cells contained 2 or 4 chromosome equivalents, while only 60% and 57%, respectively, of the wildtype cells contained 2 or 4 chromosome equivalents (Fig 7).
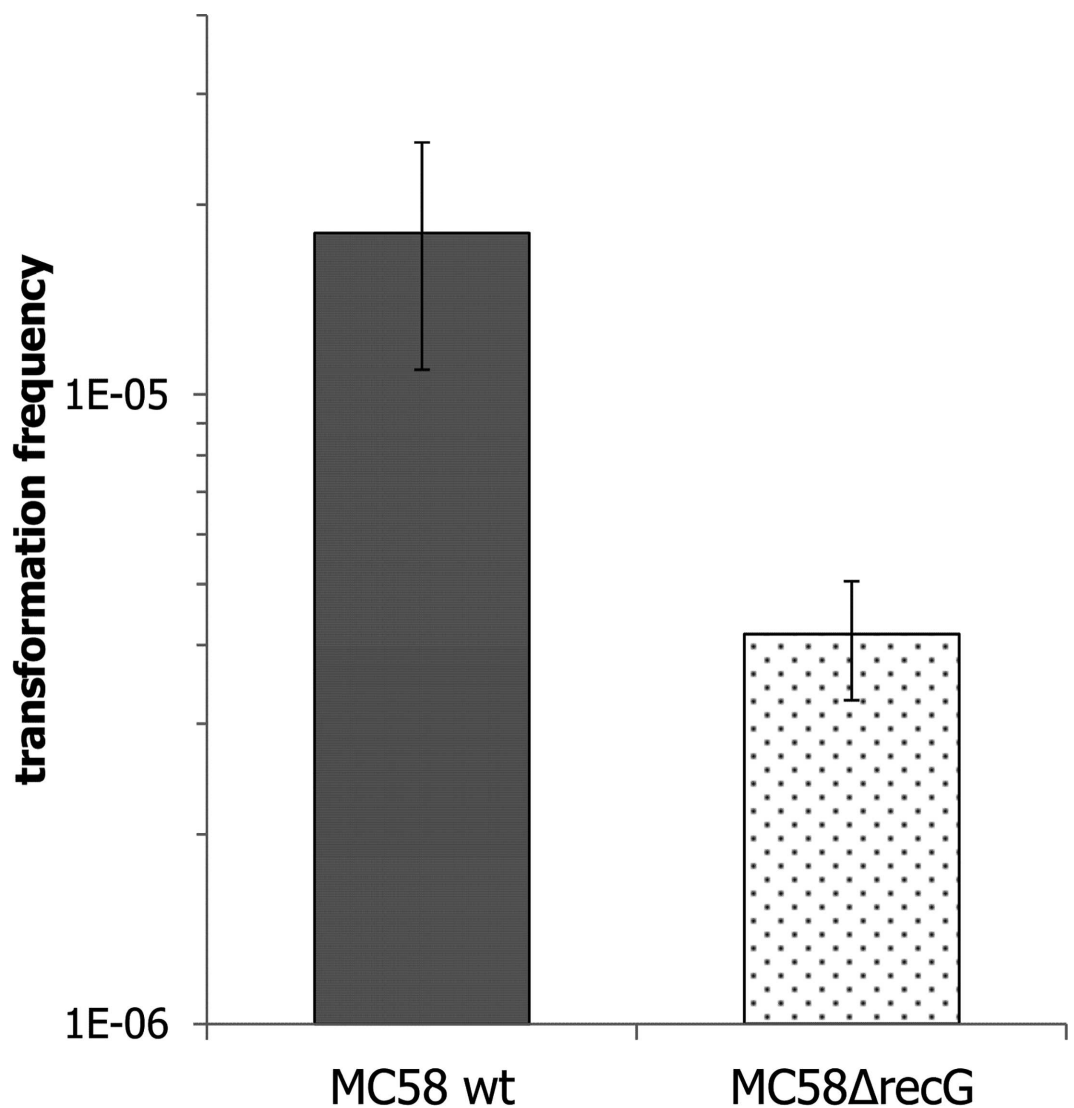

Fig 6. DNA transformation is reduced in Δ*recG* mutant. Quantitative transformation of *Neisseria meningitides* with DUS-containing plasmid DNA. The standard deviations of the median from 3 independent experiments are indicated by bars. The values on the Y- axis are in logarithmic scale. Five agar plates were inoculated from each sample.

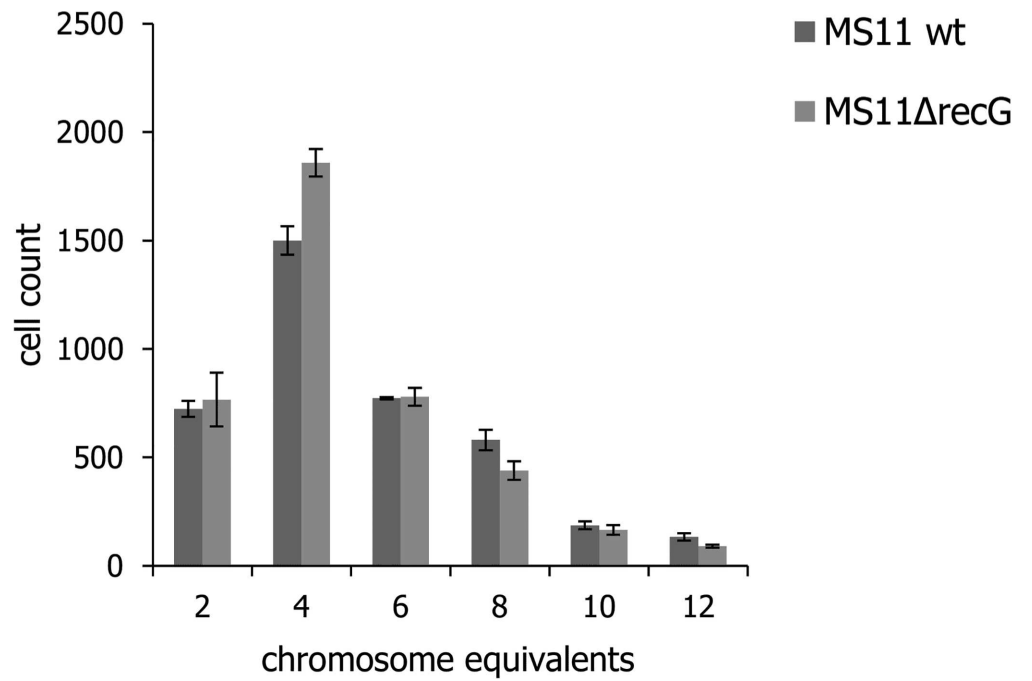doi:10.1371/journal.pone.0164588.g006

A
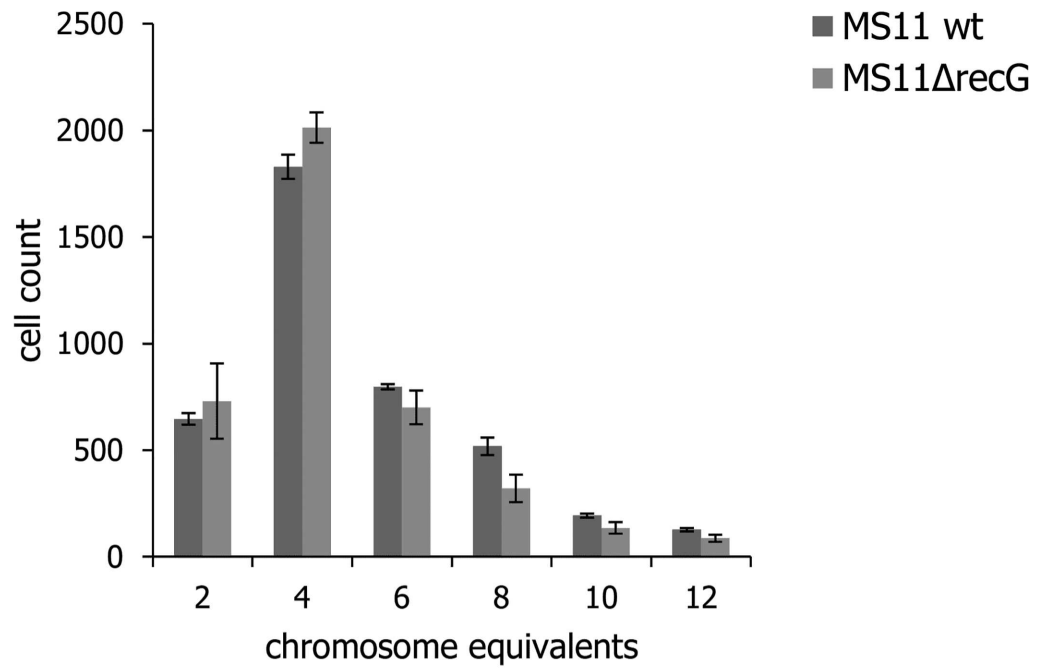
B

Fig 7. Distribution of *Neisseria gonorrhoeae* MS11 wildtype and ΔrecG mutant cells in flow cytometry analysis.
Flow cytometry of Hoechst-stained, fixed bacterial cells was performed. The x-axis shows fluorescence levels, which indicates the amount of DNA content per particle counted. Genome equivalents were determined from the stationary phase and rif-treated cells. The graphs represent the distribution of MS11 wildtype and ΔrecG mutant strains, A. from the exponential culture, B. treated with rifampicin and cephalexin acquired by selecting/gating the sub-population of cells/particles with fluorescence level corresponding to chromosome equivalents of 2, 4, 6, 8, 10 and 12.

doi:10.1371/journal.pone.0164588.g007

Nm MC58 Δ*recG* mutant cells are sensitive to genotoxic agents

Survival of $\Delta recG_{Nm}$ mutant was investigated in the presence of hydrogen peroxide, paraquat, MMS, MMC or UV radiation. Nm Δ*recG* cells were 6-fold more sensitive to paraquat, 7- and 8-fold more sensitive to MMS or MMC treatment than wildtype (Fig 8A) and also more sensitive to UV-irradiation than wildtype (2% survival vs 46% survival after exposure to 20 J/m^2 UV. Higher doses of UV killed all Δ*recG* mutant cells (Fig 8B). $\Delta recG_{Nm}$ wildtype and mutant cells were approximately equally sensitive to hydrogen peroxide (Fig 8A).

DNA uptake sequence and single nucleotide polymorphism in *recG* in the pathogenic Neisseria

Neisserial genomes carry about 2000 copies of the 10 bp DUS motif, 5'-GCCGTCTGAA-3' [50–52], which facilitates DNA binding and uptake during genetic transformation between neisserial cells. At least one DUS in the donor DNA is required for efficient transformation of DNA [53]. Comparative sequence analysis of 14 neisserial genome sequences from the public domain data [42] showed that $recG_{Nm}$ harbours five DNA uptake sequences (DUS) in the coding sequence with additional two DUS in the immediate upstream region and one DUS in the immediate downstream region (Fig 9A), making it the DUS-richest Nm gene recognized. Among the 5 DUS present in the coding region, three were located in the wedge domain and two were located in the immediate vicinity of the helicase motifs Ib and IV.

Database searching of the available Nm genomes also identified 49 single nucleotide polymorphisms (SNPs) in $recG_{Nm}$, and 37 of them were non-synonymous SNPs (nsSNPs) in the predicted $recG_{Nm}$ (Fig 9B). Seven of the nsSNPs are located in the codons for conserved active site residues of $RecG_{Nm}$, including in the wedge, ATP-binding and C-terminal helicase domains (Fig 9B). Using SNAP2 to predict functional effects of the nsSNPs [54], it appears that amino acid substitutions at positions 17, 342, 344 and 438 (S4 Table) may alter RecG function, while the remaining 33 nsSNPs are predicted to be functionally neutral or conservative.

The $RecG_{Nm}$ three-dimensional structure was modelled and SNPs mapped onto the molecular surface (Fig 9C). $RecG_{Nm}$ has typical helicase domains linked to a ´wedge´ domain and shows very little variation in the helicase motifs, with only one parsimony-informative site.

The Nm wildtype and Δ*recG* mutant strains show unique protein expression profiles

In order to identify genes that might be co-regulated with *recG*, the protein expression signatures of Nm wildtype and Δ*recG* cells were evaluated by mass spectrometry (Fig 10A). In the Nm MC58 wildtype, 1060 proteins were identified while 1064 proteins were identified in Nm MC58 Δ*recG* (Fig 10A). A list of all Nm differentially expressed (DE) proteins is given in S5 and S6 Tables. Relative to wildtype, 83 proteins were DE (29 upregulated and 54 downregulated) in the Δ*recG* strain (Table 2). The type 4 pilus structural subunit protein PilE and the minor pilin protein PilX (NMB0889) were significantly downregulated in Nm Δ*recG*, while other pilus biogenesis components (PilF, PilT and PilQ) were downregulated to a lesser extent (Table 2). Using BlastKOALA, 43 of the 83 DE proteins could be functionally categorized
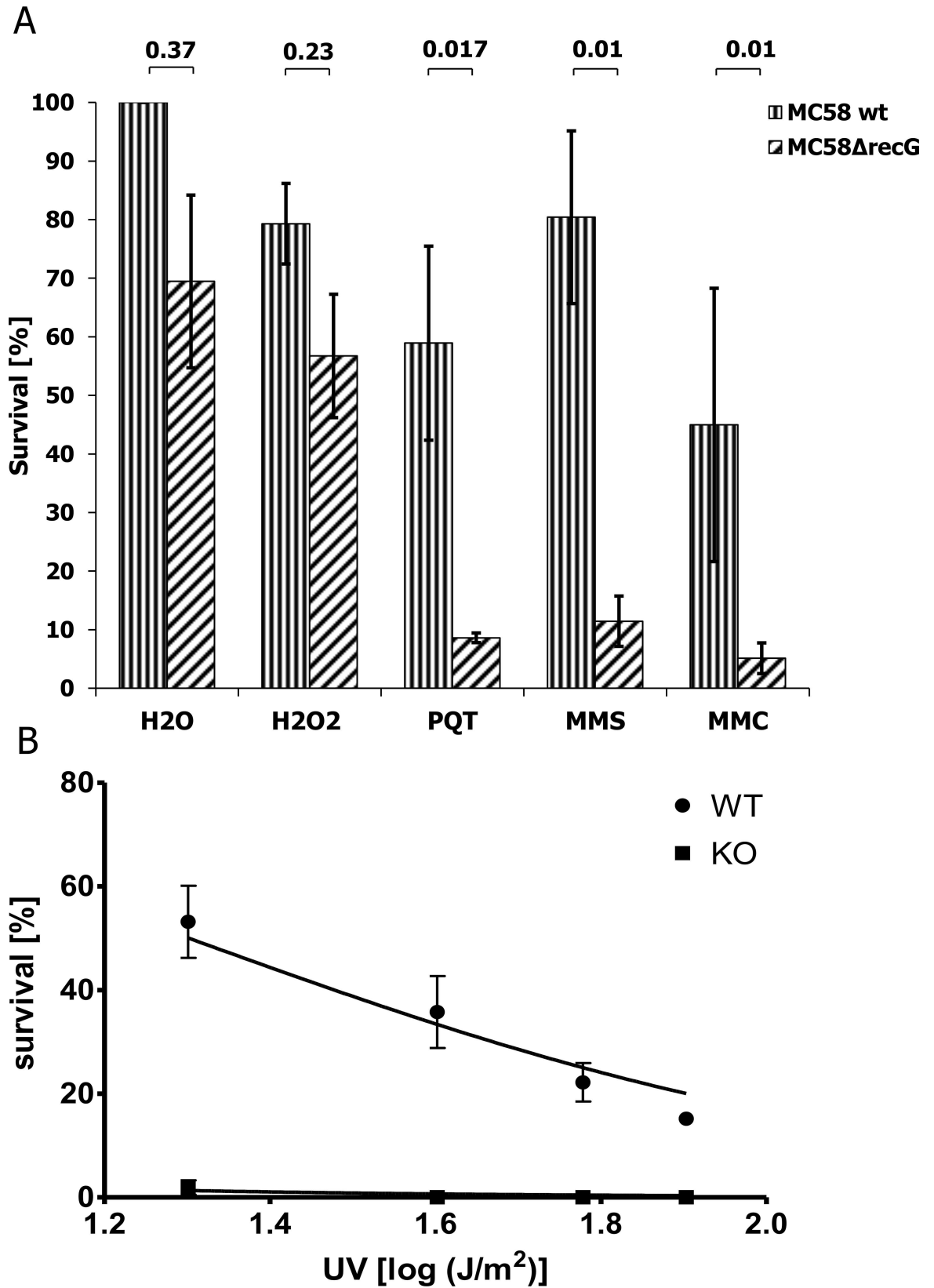
Fig 8. Alkylating agent, DNA cross linker and UV light affect the survival of a *Neisseria meningitidis* Δ*recG* mutant. A. *N. meningitidis* (Nm) MC58 wildtype and MC58Δ*recG* mutant were treated with hydrogen peroxide, paraquat, MMS and MMC. B. Survival rate of Nm MC58 wildtype and MC58Δ*recG* was determined after exposing the cells to the indicated UV influences. The standard deviations of the median from 3 independent experiments are indicated by bars.

doi:10.1371/journal.pone.0164588.g008

based on KEGG orthology (Fig 10B). The category of 3R proteins included RecN, SSB, DnaX, and the site-specific recombinase Gcr which were upregulated in the Δ*recG* mutant (Fig 10B and S6 Table). In addition, superoxide dismutase [Cu-Zn] (SodC) and the universal stress protein (USP, NMB1500) were upregulated in the Nm MC58 Δ*recG* mutant (S6 Table). The remaining 11 downregulated proteins were mainly ribosomal components involved in translation (Fig 10B).

RecG directly interacts with SSB

Gel filtration chromatography was used to test if there was an interaction between RecG$_{Nm}$ and SSB$_{Nm}$. For this experiment, RecG was pre-incubated with 2X molar excess of SSB prior to gel filtration chromatography on Superdex 200 (Fig 11). Fractions were collected and analyzed by SDS-PAGE (Fig 11, lower panel). When RecG$_{Nm}$ and SSB$_{Nm}$ were mixed before injection on the column, a new peak of the RecG$_{Nm}$:SSB$_{Nm}$ complex appeared that eluted from $\approx$ 11.2 to 13 ml earlier than the individual peaks alone; and the SSB$_{Nm}$ tetramer [55] eluted between 12 to 13.5 ml buffer (Fig 11A), indicating that RecG$_{Nm}$ and SSB$_{Nm}$ directly interact. Former reports showed that SSB interaction with RecG in *E. coli* is mediated by the last eight C-terminal amino acid residues [56,57]. Thus, when performing the same experiment with SSB$_{Nm}$ that lacks the last eight C-terminal amino acids (SSB$_{Nm\Delta C8}$), the peak formed by the RecG$_{Nm}$: SSB$_{Nm}$ complex (Fig 11A) was significantly reduced in the RecG$_{Nm}$:SSB$_{Nm\Delta C8}$ complex (Fig 11B). The reduced RecG$_{Nm}$ and SSB$_{Nm\Delta C8}$ interaction confirmed the necessity of the 8 C-terminal residues of SSB$_{Nm}$ for the interaction with RecG$_{Nm}$. The interaction between RecG$_{Nm}$ and SSB$_{Nm}$ was also confirmed by MST, with SSB$_{Nm}$ as the labelled molecule and RecG$_{Nm}$ as the ligand, indicating a K$_d$ value of 558 ±139 nM for this reaction (Fig 11C).

Discussion

RecG is a double-stranded DNA translocase and helicase thought to play multiple roles in cellular processes including initiation of origin-dependent DNA replication, remodelling, regressing and restarting replication forks stalled at DNA lesions [22,58]. Previous studies show that RecG binds and unwinds a variety of branched model substrates that resemble stalled DNA replication, repair and recombination intermediates [7,20,59]. *In vitro*, *E.coli* RecG preferentially unwinds a fork-like DNA substrate with a single-stranded leading arm [22,60], where remodelling of branched intermediates by RecG through homologous recombination plays a fundamental role in directing DNA synthesis and thus maintaining genomic stability [61]. This study shows that RecG$_{Nm}$ binds and unwinds HJ structure, replication forks and D-loops in the presence of ATP, which is consistent with the proposed roles of RecG$_{Nm}$ in DNA repair, DNA replication and homologous recombination [13,60,62]. Similar to the *E. coli* RecG, RecG$_{Nm}$ displayed ATPase activity, however, with equivalent efficiency of ATP hydrolysis with either of the DNA cofactors employed (Fig 4). The preferred co-factor for the *E. coli* RecG ATPase activity is negatively-supercoiled DNA for the unbranched DNA [24] and HJ for branched DNA substrates [24,56,63].

We have shown that more than one third of the colonies formed by the Nm Δ*recG* null mutant are small and non-agglutinating (Fig 5B and 5C), suggesting that this mutant has a lower growth rate than the wildtype. Consistent with this, Sechman et al (2006) showed that
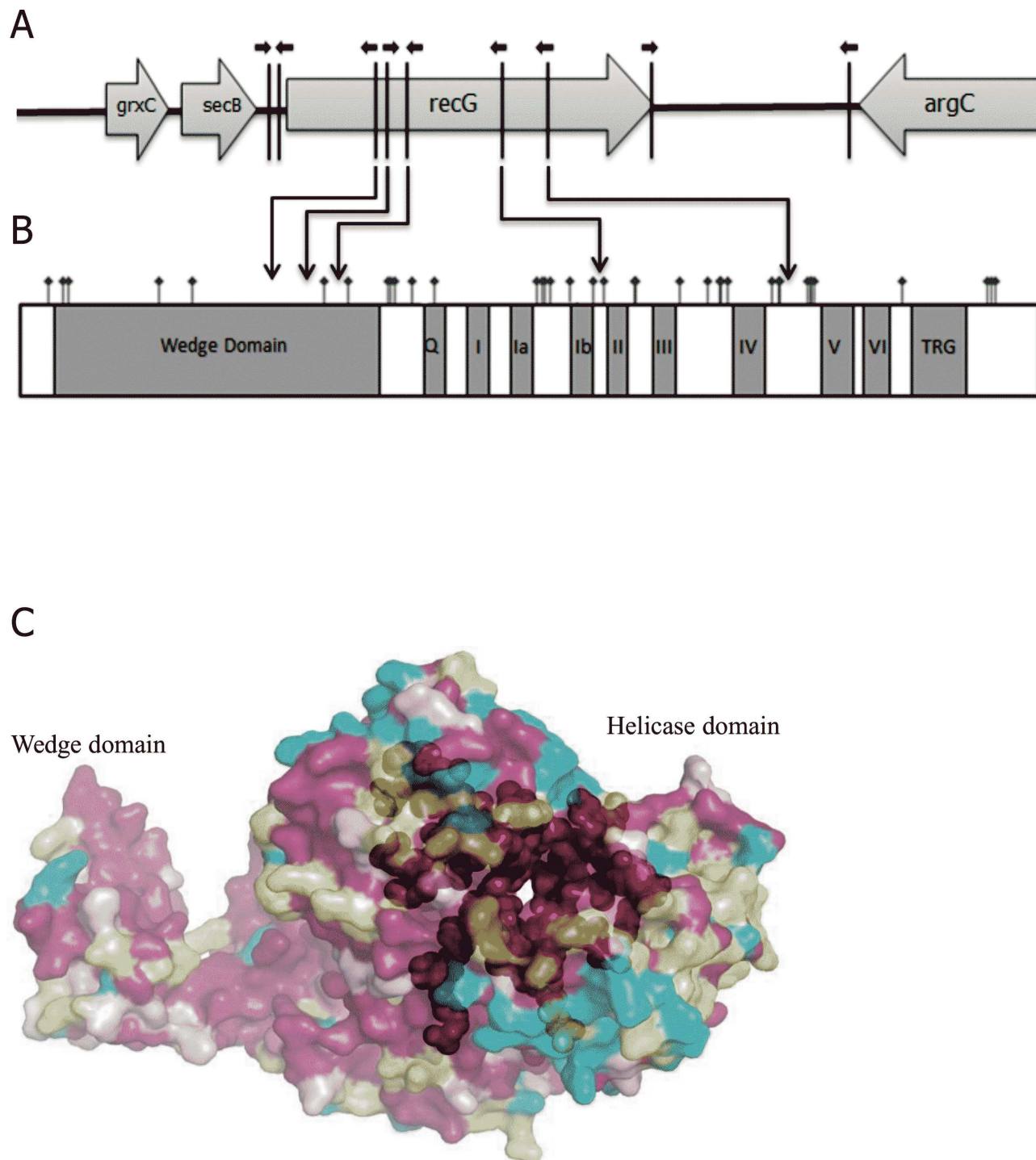
Fig 9. Neisseria meningitidis recG (recG$_{Nm}$) is a DNA uptake sequence (DUS) abundant gene. A. Schematic diagram of the *N. meningitidis* (Nm) *recG* gene (*recG$_{Nm}$*) and neighbouring genes showing the position of the DNA uptake sequences (DUS) (black arrows). B. Domain organization in the RecG$_{Nm}$ and non-synonymous single nucleotide polymorphism (nsSNP) identified in *recG$_{Nm}$* from different Nm strains. The positioning of the nsSNPs is shown in square tick marks (bold). C. The predicted structure of RecG$_{Nm}$ with colour coding for conserved (red) and variable (blue) regions, yellow regions indicate insufficient data. The RecG$_{Nm}$ regions outside of the helicase motifs are shown in transparent.

doi:10.1371/journal.pone.0164588.g009
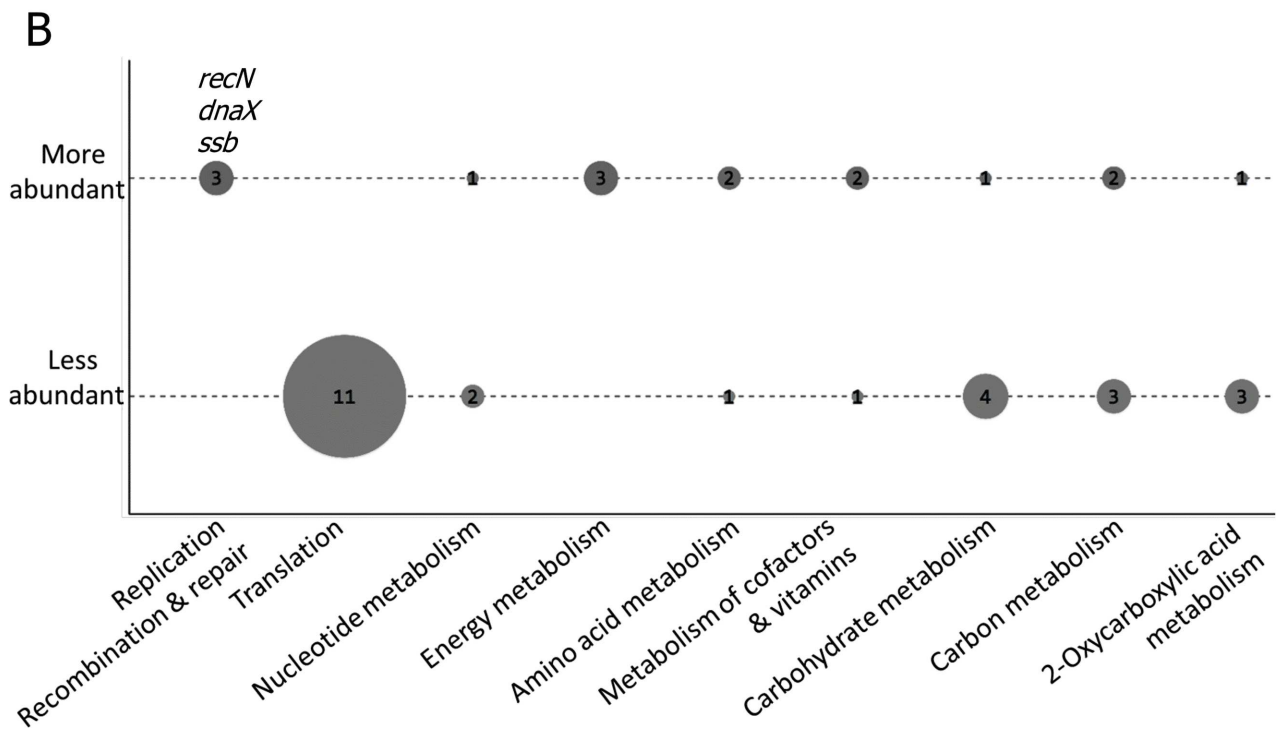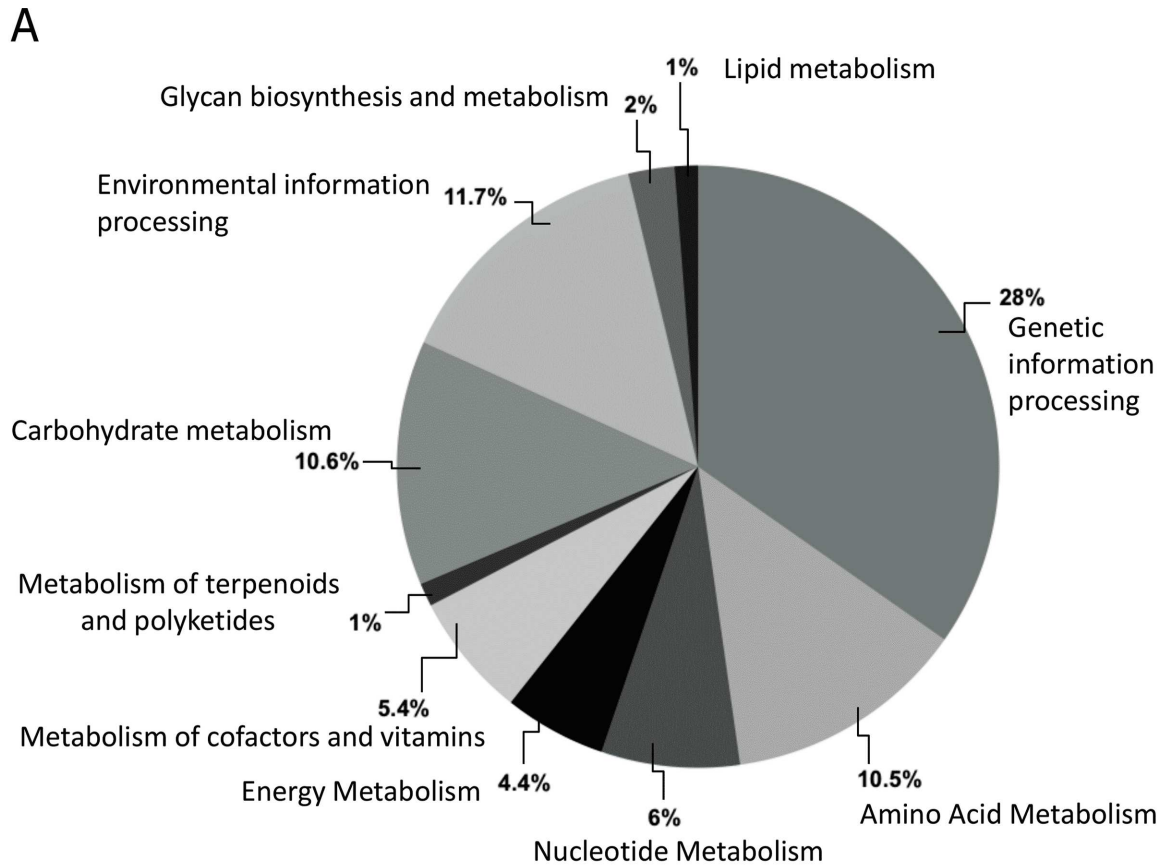
Fig 10. Functional classification of proteins identified and differentially expressed in _Neisseria meningitidis_ by mass spectrometry. A. Pie-chart representing the functional classification of all identified proteins identified using high-resolution mass spectrometry. The 1073 proteins were distributed in 10 functional categories based on KEGG orthology using BlastKOALA. B. Differentially more abundant and less abundant proteins in Nm wildtype and NmΔ_recG_ sorted by KEGG where the dot plot size is proportional to the counts of differentially expressed (DE) proteins.

doi:10.1371/journal.pone.0164588.g010

both the RecG and RuvABC HJ processing pathways are required for recombinational repair and for normal growth when RecA is expressed [14]. The ribosome efficiency and the amount of ribosomal protein per genome decreased with decreasing growth rate in an _E. coli_ universal stress protein (USP) mutant [64]. This result in Nm was supported by the mass spectrometry profiling of the Δ_recG_ mutant compared to the wildtype. In fact, in Δ_recG_$_{Nm}$ cells, 11 ribosomal proteins were less abundant as compared to the wildtype (Fig 10B), which might explain the growth defect. Also, the _E. coli_ USP homologue NMB1500 was significantly upregulated in the Nm Δ_recG_ mutant (S5 Table), and _E. coli_ USP was shown to be induced in response to stress causing cell growth-arrest [65]. The reduced expression of the type 4 pilus structural subunit protein PilE, PilX as well as the type 4 pilus biogenesis components (PilF, PilT and PilQ) in Δ_recG_$_{Nm}$ mutant cells is also consistent with the non-agglutinating colony morphology and phenotypes observed. Nm mutants of the _pilQ_ [30], _pilE_ [66], _pilT_ [67] and _pilG_ [68] genes were reported to be transformation deficient. The minor pilin protein PilX is involved in Nm pathogenesis, essential for aggregation and adhesion to host tissues [69].

The initiation of additional replication forks in _E. coli_ Δ_recG_ mutants leads to head to head collision of forks moving in opposite directions, which in turn contributes to the formation of secondary replication forks [10]. This cycle of generating new replication forks results in the accumulation of branched DNA intermediates which interfere with normal DNA replication and make cells defective in chromosome segregation [10]. We hypothesized that in neisserial Δ_recG_ mutant cells, their DNA replication is hindered due to the accumulation of branched DNA structures, which would leave the cells with a reduced number of fully replicated chromosomes compared to the wildtype. However, in this study, flow cytometry assay showed no significant difference with regards to the number of active replication forks between Ng wildtype and Δ_recG_ mutant cells (S7 Fig) and no biologically detectable role for RecG$_{Nm}$ in replication was found.

The Nm Δ_recG_ mutant was sensitive to paraquat, MMS, mitomycin C and UV radiation, but relatively insensitive to hydrogen peroxide, as are _Neisseria_ species in general [70]. Although both H_2O_2 and paraquat cause oxidative damage, the damage due to paraquat is more severe than the damage caused by H_2O_2 [71]. This is because paraquat not only causes oxidative damage via O_2^-, but also keeps it on the cycle of production of HO^- from H_2O_2 by increasing the availability of Fe^{2+} [72]. RecG seems to play a vital role when exposed to paraquat as opposed to hydrogen peroxide. The resistance of Nm Δ_recG_ to H_2O_2 might be attributed to the upregulation of Gcr, RecN and SodC (S6 Table) [73]. Unlike the Nm Δ_recG_ mutant, an Ng Δ_recG_ mutant in a previous study was susceptible to H_2O_2 exposure [74]. In a former microarray analysis of Ng wildtype exposed to H_2O_2, _recN_ was the sole gene upregulated compared to other DNA-repair and recombination enzymes [74]. Site-specific recombinases are involved in the control of gene expression, generation of genetic diversity, and separation of dimeric chromosomes; in fact, HJ is the main intermediate for their function [53]. The periplasmic or outer-membrane anchored protein SodC is hypothesized to protect pathogenic bacteria from reactive oxygen species (ROS) of the outside sources, from immune cells [75].

UV-irradiated _E. coli_ Δ_recG_ mutant cells form replication forks outside the origin of replication (oriC) [76], and _recG_-deficient _E. coli_ cells are sensitive to fork-blocking agents [77,78]. Nm Δ_recG_ cells were sensitive to both MMC and MMS (Fig 8). In _E. coli_, alpha-ketoglutarate-

Table 2. The list of differentially expressed proteins involved in DNA replication, recombination and repair and neisserial type IV pilus biogenesis.

Protein fold	Protein name	Gene name
	Replication, recombination and repair proteins	
2,58	DNA repair protein RecN	recN*
1,36	DNA polymerase III, subunits gamma and tau	dnaX*
3,62	Site-specific recombinase	gcr*
1,75	Single-stranded DNA-binding protein	Ssb*
-3,60	DNA helicase	uvrD
-3,35	UvrABC system protein B	uvrB
-1,41	Regulatory protein RecX	recX
-1,38	DnaA-related protein	NMB1076
-1,24	ATP-dependent DNA helicase RuvA	ruvA
-1,20	DNA polymerase III, delta subunit	holA
-1,18	DNA polymerase I	polA
-1,15	DNA recombination protein RmuC homolog	rmuC
-1,12	RecBCD enzyme subunit RecC	recC
-1,06	DNA gyrase subunit B	gyrB
-1,05	Recombination-associated protein RdgC	rdgC
-1,05	DNA polymerase III subunit beta	dnaN
-1,01	Protein RecA	recA
1,02	UvrABC system protein A	uvrA
1,10	DNA polymerase III, epsilon subunit	dnaQ-2
1,16	Putative ATP-dependent RNA helicase	NMB1422
1,16	DNA polymerase III subunit alpha	dnaE
1,18	Replicative DNA helicase	dnaB
1,18	DNA gyrase subunit A	gyrA
1,24	ATP-dependent DNA helicase RuvB	ruvB
1,30	MutT protein	mutT
1,47	DNA topoisomerase 4 subunit A	parC
1,51	DNA topoisomerase 1	topA
1,68	DNA mismatch repair protein MutS	mutS
2,66	RecBCD enzyme subunit RecD	recD
4,44	DNA topoisomerase 4 subunit B	parE
	Type 4 pilus biogenesis components	
-2,69	Fimbrial protein	pilE*
-3,67	Type 4 pilus assembly protein	NMB0889 (pilX)*
-1,38	Twitching motility protein PilT	pilT-1
-1,13	Putative type 4 pilus assembly protein PilZ	NMB0770
-1,05	Type 4 pilus biogenesis and competence protein PilQ	pilQ
1,01	Twitching motility protein PilT	pilT-2
1,09	PilO protein	pilO
1,14	PilM protein	pilM
1,19	PilN protein	pilN
1,31	PilP protein	pilP
1,44	Pilus assembly protein PilG	pilG
1,88	Type IV pilus assembly protein	pilF
-1,03	Twitching motility protein	NMB0051

The minus sign of the protein fold change indicate the downregulated whereas the positive sign shows upregulated proteins. Protein fold changes are log2-transformed t-test difference values.

* Significantly downregulated proteins in Nm in *recG* mutant

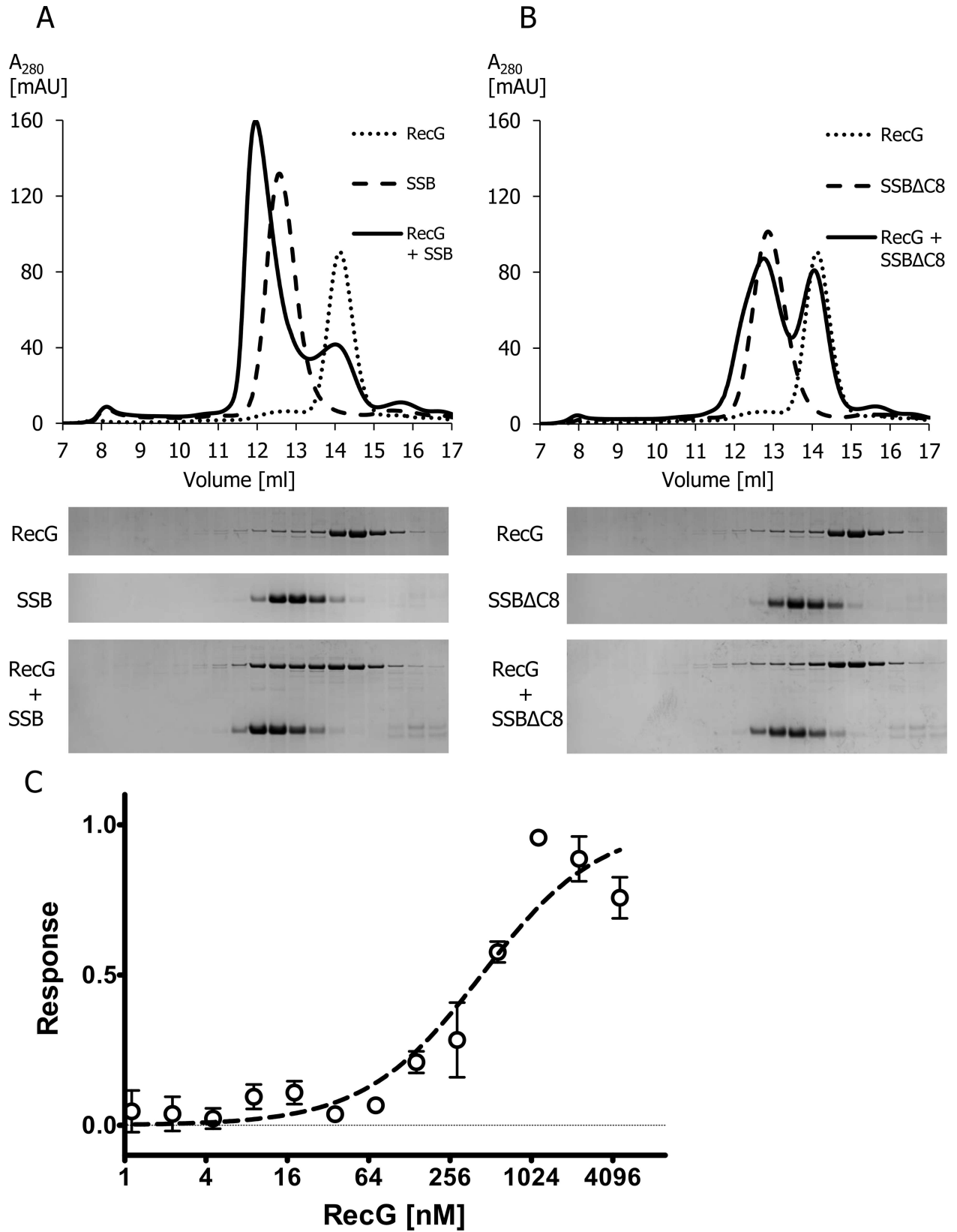doi:10.1371/journal.pone.0164588.t002

Fig 11. RecG_Nm directly interacts with SSB_Nm. A. Co-gel filtration analysis was performed to monitor the interaction between of RecG_Nm and SSB_Nm. Upper panels: chromatogram A_{280} [mAU] vs retention volume [ml]. Lower panels: SDS-PAGE of 13μl sample from each 0.5ml fraction beginning from 9.5 ml up to 16 ml, and stained with Coomassie blue. A. 20 μM RecG_Nm mixed with 40 μM SSB_Nm and each protein alone. B. 20 μM RecG_Nm mixed with 40 μM SSB_NmΔC8 and each protein alone. C. Microscale thermophoresis (MST) analysis of the interaction between RecG_Nm and SSB_Nm. MST results of three independent experiments were included. The average and standard deviation of the normalised response and the fitted curve are shown. The calculated Kd value of the interaction is 558 ±139 nM.

doi:10.1371/journal.pone.0164588.g011

dependent dioxygenase (AlkB) promotes repair of alkylation damage to DNA [79]. However, an Nm homolog of AlkB has not been identified [2]. The binding and unwinding of the RecG_Nm to model substrates that mimics an arrested DNA replication fork may suggest that RecG_Nm also promotes the rescue of alkylation induced replication fork arrest. When a replication fork is arrested, a single strand gap is introduced into the leading strand which is an ideal substrate for RecG [22]. *E. coli recG* mutants are sensitive to MMS [80] and the loss of *recG* can be complemented by *recG* from *Mycobacterium tuberculosis*, restoring the ability to repair MMS-, MMC- and UV-induced DNA damage [59].

In our hands, Nm *ΔrecG* cells were extremely sensitive to UV-irradiation with 20-fold lower survival rate than wildtype cells (Fig 8B). This finding conflicts with an earlier report on *E. coli* where inactivation of RecG resulted only in moderate sensitivity to UV [78]. This difference might be explained by the fact that *E. coli* expresses photolyase, while the *Neisseria* species do not [81]. DNA photolyases are monomeric, light-driven enzymes dedicated to revert lethal UV light-induced DNA damage [82,83]. This would explain the greater role of *recG* in protecting the Nm genome against UV-induced DNA damage. Tønjum and colleagues [2] suggested that nucleotide excision repair (NER) might be the main pathway for repair of UV-induced DNA lesions in *Neisseria*. They also showed that the Nm *uvrA* mutant exhibits a 30,000-fold lower survival than wildtype after exposure to 20 J/m² UV-irradiation [84]. UvrA is part of the endonuclease system involved in the nucleotide excision repair pathway together with UvrB and UvrC [85,86]. It is conceivable that RecG facilitates the repair of DNA lesions by NER by regressing a stalled fork and allowing NER enzymes access to a DNA lesion within duplex DNA [60,87,88]. Hence, it would be interesting to study the ability of NER-deficient RecG mutants to recover from exposure to UV.

As previously reported [14,89], reduced competence for transformation has been observed in MC58*ΔrecG* mutants (Fig 6) when the cells were exposed to DNA for a limited time (15 min). With continuous exposure to DNA over longer time, *ΔrecG* mutant cells demonstrated comparable transformability with the wildtype strain (S6 Fig). Equivalent transformability of *ΔrecG* mutant cells and wildtype cells when the DNA incubation lasted for more than 30 min, might be due to other helicases can compensate the *recG* function as a back-up during genetic transformation; this also suggests that the reduced transformability of *ΔrecG_Nm* cells at 15 min exposure was not due to a viability problem. Transformation in Ng was severely lowered in the double mutants of *recG* and *ruvA* or *ruvB* strains, whereas *ruvA* and *ruvB* double mutants were transformable equivalent to the wild type [14]. Hence, it is tempting to speculate that RecG_Nm is a preferred enzyme within the recombinational repair pathway. Consistent with this idea, it has been reported that the precise structure of a stalled replication fork dictates the kinetics of restart and repair [56]. For instance, when the stalled replication fork includes an exposed region of ssDNA, the SSB first loaded on to ssDNA. The RecG is then recruited prior to recruiting RuvAB [56]. In this context, we have shown that RecG_Nm directly interacts with SSB (Fig 11), and SSB is more abundant in the *ΔrecG* mutant than the wildtype as assessed by MS data (S6 Table).

This study also shows that *recG_Nm* harbors an unusually high density of DUS [53], rendering *recG* with the highest number of DUS inside a single gene (Fig 9A), while *mutY* is the most DUS-dense gene recognized in terms of number of DUS per nucleotides [52]. It has been

observed that the number and density of DUS is significantly higher in neisserial genes involved in DNA repair, recombination, restriction-modification and replication than in any other gene group [52]. This is consistent with the idea that DUS enhance the probability of DNA uptake, and that there might be selective advantage in efficient uptake of a gene involved in genome maintenance and the response to genotoxic stress [52].

A somewhat unexpected finding was the presence of a high number of nsSNPs in $recG_{Nm}$ where one fifth of the nsSNPs were located in functional motifs, including those encoding the wedge, ATP-binding and C-terminal helicase domains. This might contribute to the $RecG_{Nm}$ adaptive potential. In contrast, *M. tuberculosis* RecG [90] is highly conserved and very few SNPs in $recG_{Mtb}$ have been reported to date.

Collectively, these studies on Nm RecG provide insight into its role in DNA repair, recombination and the induction of a phenotypically detectable growth defect, while its potential function in replication requires additional studies.

Supporting Information

S1 Fig. Purification of 6xhis-tagged Nm RecG. Lanes 1, Marker SeeBlue® Plus2 standard, 2, lysate of uninduced bacterial culture, 3, induced control cell lysate (0.5mM IPTG), 4, whole cell lysate, 5, pellet of whole cell lysate, 6, cleared lysate, 7 & 8, 2x wash with 20mM imidazole, 9, wash with 40mM imidazole, 10, flow-through of an Ni^2-NTA-agarose column, 11–16, elution from Ni^2-NTA-agarose with 80mM, 120mM, 160mM, 200mM (2x) and 250mM imidazole, respectively.
(TIF)

S2 Fig. Quantitation of the gel images of the *Neisseria meningitidis* RecG DNA unwinding assay. A. Holliday junction. B. Fork substrates. The data presented are the means of ± SD from 3 independent experiments.
(TIF)

S3 Fig. $RecG_{Nm}$ binds D-loop substrates. Representative gel images from 3 independent experiments. i) 5′ hairpin tail D-loop, ii) 5′ tail D-loops, and iii) 3′ tail D-loop. Lanes: 1) no protein, 2) 200 nM $RecG_{Nm}$, 3) 400 nM $RecG_{Nm}$, 4) 400 nM $RecG_{Nm}$K294A.
(TIF)

S4 Fig. $RecG_{Nm}$ unwinds D-loops. Representative gel images from 3 independent experiments. i) 5′ hairpin tail D-loop, ii) 5′ tail D-loop, and iii) 3′ tail D-loop DNA substrates. Lanes: 1) no protein, 2) 200 nM $RecG_{Nm}$, 3) 400 nM $RecG_{Nm}$, 4) 400 nM $RecG_{Nm}$K294A. The Δ designates boiled substrate.
(TIF)

S5 Fig. Gel images of ATPase activity of $RecG_{Nm}$ and $RecG_{Nm}$K294A from three independent experiments. A. i) AM13mp18 ssDNA and ii) pET28b(+) dsDNA. B. i) Single-stranded 80 nucleotides polyT. ii) Double-stranded 80 nucleotides polyAT. C. i) Single-stranded 100 nucleotide polyT. ii) Double-stranded 100 nucleotides polyAT. (–) is reaction with no protein, (wt) is wildtype protein ($RecG_{Nm}$), (K294A) is $RecG_{Nm}$K294A.
(TIF)

S6 Fig. *Neisseria meningitidis* wildtype and Δ*recG* mutant cells exhibit equivalent DNA transformation frequencies with exposure to DNA for 30 min. Quantitative transformation of *N. meningitidis* MC58 wildtype and Δ*recG* mutant with DUS-containing plasmid DNA. The standard deviations of the median from four independent experiments are indicated by bars. Three replicates were inoculated from each sample.
(TIF)

S7 Fig. Flow cytometry analysis of *Neisseria gonorrhoeae* cells. Flow cytometry of Hoechst-stained, fixed bacterial cells was performed. For each histogram, the x-axis shows fluorescence levels, which indicates the amount of DNA content per particle counted. The y-axis shows counts, which indicates the number of fluorescing particles or cells. The overlay of sub-population of cells (shaded in black) acquired by gating cells with fluorescence level corresponding to chromosome equivalents of 2, 4, 6, 8, 10 and 12, and the parental histogram (contour). Genome equivalents were determined from the stationary phase and rif-treated *E. coli* and are shown in the lower panel (panel V). The X-axis designates the fluorescence intensity in the blue channel, representing the amount of DNA per particle counted. i) *Neisseria gonorrhoeae* (g) MS11 wild-type strain and iii) Ng MS11Δ*recG* mutant strain from the exponential culture, and ii) Ng MS11 wildtype and iv) Ng MS11Δ*recG* mutant strains continued to grow for additional six hours in the presence of 40 μg ml^{-1} rifampicin and 4 μg ml^{-1} cephalexin. V) Slowly growing *Escherichia coli* CM735 stained with Hoechst 33258 was used as standard to calibrate the flow cytometer, as the *E. coli* 4.6 Mb chromosome is similar to an Ng diplococcus of 2.3 Mb chromosomes.
(TIF)

S1 Table. The list of primers employed in the study.
(DOCX)

S2 Table. DNA Oligonucleotides employed in this study.
(DOCX)

S3 Table. *Neisseria meningitidis* does not exhibit a defect in replication. The DNA content and cell mass of individual *Neisseria gonorrhoeae* wildtype and Δ*recG* mutant cells derived from flow cytometry analysis.
(DOCX)

S4 Table. *Neisseria meningitidis* amino acid variation. The position of amino acids encoded by non-synonymous single nucleotide polymorphisms (nsSNPs) identified in the deduced RecG protein of *Neisseria meningitidis*.
(DOCX)

S5 Table. Significantly down-regulated proteins in *Neisseria meningitidis* MC58 Δ*recG*. Differentially less abundant proteins in *Neisseria meningitidis* (Nm) MC58 Δ*recG* as compared to the Nm MC58 wildtype, sorted according to fold change. Protein fold changes are log2-transformed t-test difference values.
(DOCX)

S6 Table. Significantly up-regulated proteins in *Neisseria meningitidis* MC58 Δ*recG*. Differentially more abundant proteins in *Neisseria meningitidis* (Nm) MC58 Δ*recG* as compared to the Nm MC58 wildtype, sorted according to fold change. Protein fold changes are log2-transformed t-test difference values.
(DOCX)

Author Contributions

Conceptualization: TT GTB SVB SAF HH.

Data curation: TT GTB TR SK AN.

Formal analysis: TT GTB SAF TR SK AN.

Funding acquisition: TT.

Investigation: TT GTB SVB SAF TR SK HH.

Methodology: TT GTB SVB SAF TR SK HH AN.

Project administration: TT SVB.

Resources: TT.

Software: GTB AN TR SK.

Supervision: TT.

Validation: TT GTB SVB SAF TR SK HH AN.

Visualization: TT GTB SK AN HH.

Writing – original draft: TT GTB SVB SAF.

Writing – review & editing: TT GTB SVB.

References

1. Nassif X (2000) Microbiology. A Furtive Pathogen Revealed. Science (80-) 287: 1767–1768. doi: 10.1126/science.287.5459.1767 PMID: 10755929

2. Davidsen T, Tønjum T (2006) Meningococcal genome dynamics. Nat Rev Microbiol 4: 11–22. doi: 10.1038/nrmicro1324 PMID: 16357857

3. Black CG, Fyfe JA, Davies JK, Black CG, Janet AM, Fyfe JKD (1998) Absence of an SOS-like system in Neisseria gonorrhoeae. Gene 208: 61–66. PMID: 9479048

4. Nagorska K, Silhan J, Li Y, Pelicic V, Freemont PS, Baldwin GS, et al. (2012) A network of enzymes involved in repair of oxidative DNA damage in Neisseria meningitidis. Mol Microbiol 83: 1064–1079. doi: 10.1111/j.1365-2958.2012.07989.x PMID: 22296581

5. Brosh RM (2013) DNA helicases involved in DNA repair and their roles in cancer. Nat Rev Cancer 13: 542–558. doi: 10.1038/nrc3560 PMID: 23842644

6. Rocha EPC, Cornet E, Michel B (2005) Comparative and evolutionary analysis of the bacterial homologous recombination systems. PLoS Genet 1: e15. doi: 10.1371/journal.pgen.0010015 PMID: 16132081

7. Zegeye ED, Balasingham SV, Laerdahl JK, Homberset H, Tønjum T (2012) Mycobacterium tuberculosis RecG binds and unwinds model DNA substrates with a preference for Holliday junctions. Microbiology 158: 1982–1993. doi: 10.1099/mic.0.058693–0 PMID: 22628485

8. Wallet C, Le Ret M, Bergdoll M, Bichara M, Dietrich A, Gualberto JM (2015) The RECG1 DNA Translocase Is a Key Factor in Recombination Surveillance, Repair, and Segregation of the Mitochondrial DNA in Arabidopsis. Plant Cell 27: tpc.15.00680. doi: 10.1105/tpc.15.00680 PMID: 26462909

9. Mahdi AA, Briggs GS, Sharples GJ, Wen Q, Lloyd RG (2003) A model for dsDNA translocation revealed by a structural motif common to RecG and Mfd proteins. EMBO J 22: 724–734. doi: 10.1093/emboj/cdg043 PMID: 12554672

10. Rudolph Christian J., Upton AL, Harris L, Lloyd RG (2009) Pathological replication in cells lacking RecG DNA translocase. Mol Microbiol 73: 352–366. doi: 10.1111/j.1365-2958.2009.06773.x PMID: 19538444

11. Rudolph CJ, Mahdi AA, Upton AL, Lloyd RG (2010) RecG protein and single-strand DNA exonucleases avoid cell lethality associated with PriA helicase activity in Escherichia coli. Genetics 186: 473–492. doi: 10.1534/genetics.110.120691 PMID: 20647503

12. Sharples GJ, Ingleston SM, Lloyd RG (1999) Holliday Junction Processing in Bacteria: Insights from the Evolutionary Conservation of RuvABC, RecG, and RusA. J Bacteriol 181: 5543–5550. PMID: 10482492

13. McGlynn P, Lloyd RG (1999) RecG helicase activity at three- and four-strand DNA structures. Nucleic Acids Res 27: 3049–3056. PMID: 10454599

14. Sechman EV, Kline KA, Seifert HS (2006) Loss of both Holliday junction processing pathways is synthetically lethal in the presence of gonococcal pilin antigenic variation. Mol Microbiol 61: 185–193. doi: 10.1111/j.1365-2958.2006.05213.x PMID: 16824104

15. Sun Y-HH, Exley R, Li Y, Goulding D, Tang C (2005) Identification and Characterization of Genes Required for Competence in Neisseria meningitidis. J Bacteriol 187: 3273–3276. doi: 10.1128/JB.187.9.3273 PMID: 15838056

16. Wu Y, Chen W, Zhao Y, Xu H, Hua Y (2009) Involvement of RecG in H2O2-induced damage repair in Deinococcus radiodurans. Can J Microbiol 55: 841–848. doi:w09-028 [pii]\r10.1139/w09-028. doi: 10.1139/w09-028 PMID: 19767856

17. Ochsner UA, Vasil ML, Alsabbagh E, Parvatiyar K, Hassett DJ (2000) Role of the Pseudomonas aeruginosa oxyR-recG operon in oxidative stress defense and DNA repair: OxyR-dependent regulation of katB-ankB, ahpB, and ahpC-ahpF. J Bacteriol 182: 4533–4544. PMID: 10913087

18. Benam AV, Lang E, Alfsnes K, Fleckenstein B, Rowe AD, Hovland E (2011) Structure-function relationships of the competence lipoprotein ComL and SSB in meningococcal transformation. Microbiology 157: 1329–1342. doi: 10.1099/mic.0.046896–0 PMID: 21330432

19. Gibson DG, Young L, Chuang R-Y, Venter JC, Hutchison CA, Smith HO (2009) Enzymatic assembly of DNA molecules up to several hundred kilobases. Nat Methods 6: 343–345. doi: 10.1038/nmeth.1318 PMID: 19363495

20. McGlynn P, Al-Deib A, Liu J, Lloyd RG (1997) The DNA replication protein PriA and the recombination protein RecG bind D-loops. J Mol Biol 270: 212–221. doi: 10.1006/jmbi.1997.1120 PMID: 9236123

21. Lloyd RG, Sharples GJ (1993) Dissociation of synthetic Holliday junctions by E. coli RecG protein. EMBO J 12: 17–22. PMID: 8428576

22. McGlynn P, Lloyd RG (2001) Rescue of stalled replication forks by RecG: simultaneous translocation on the leading and lagging strand templates supports an active DNA unwinding model of fork reversal and Holliday junction formation. Proc Natl Acad Sci U S A 98: 8227–8234. doi: 10.1073/pnas.111008698 PMID: 11459957

23. Brosh RM, Opresko PL, Bohr VA (2006) Enzymatic mechanism of the WRN helicase/nuclease. Methods Enzymol 409: 52–85. doi: 10.1016/S0076-6879(05)09004-X PMID: 16793395

24. Slocum SL, Buss J, Kimura Y, Bianco PR (2007) Characterization of the ATPase activity of the Escherichia coli RecG protein reveals that the preferred cofactor is negatively supercoiled DNA. J Mol Biol 367: 647–664. doi: 10.1016/j.jmb.2007.01.007 PMID: 17292398

25. Blake MS, MacDonald CM, Klugman KP (1989) Colony morphology of piliated Neisseria meningitidis. J Exp Med 170: 1727–1736. PMID: 2572672

26. Geissmann Q (2013) OpenCFU, a New Free and Open-Source Software to Count Cell Colonies and Other Circular Objects. PLoS One 8: 1–10. doi: 10.1371/journal.pone.0054072 PMID: 23457446

27. Ambur OH, Frye SA, Nilsen M, Hovland E, Tønjum T (2012) Restriction and sequence alterations affect DNA uptake sequence-dependent transformation in Neisseria meningitidis. PLoS One 7: e39742. doi: 10.1371/journal.pone.0039742 PMID: 22768309

28. Tettelin H, Saunders NJ, Heidelberg J, Jeffries AC, Nelson KE, Eisen JA, et al. (2000) Complete genome sequence of Neisseria meningitidis serogroup B strain MC58. Science 287: 1809–1815. doi: 10.1126/science.287.5459.1809 PMID: 10710307

29. Frasch CE, Chapman SS (1972) Classification of Neisseria meningitidis Group B into Distinct Serotypes I. Serological Typing by a Microbactericidal Method. Infect Immun 5: 98–102. PMID: 4632471

30. Tønjum T, Caugant DA, Dunham SA, Koomey M (1998) Structure and function of repetitive sequence elements associated with a highly polymorphic domain of the Neisseria meningitidis PilQ protein. Mol Microbiol 29: 111–124. PMID: 9701807

31. Frye SA, Nilsen M, Tonjum T, Ambur OH, Tønjum T (2013) Dialects of the DNA uptake sequence in neisseriaceae. PLoS Genet 9: e1003458. doi: 10.1371/journal.pgen.1003458 PMID: 23637627

32. Davidsen T, Bjørås M, Seeberg EC, Tønjum T (2005) Antimutator Role of DNA Glycosylase MutY in Pathogenic Neisseria Species. J BACTERIOL 187. doi: 10.1128/JB.187.8.2801

33. Balasingham SV, Collins RF, Assalkhou R, Homberset H, Frye SA, Derrick JP, et al. (2007) Interactions between the lipoprotein PilP and the secretin PilQ in Neisseria meningitidis. J Bacteriol 189: 5716–5727. doi: 10.1128/JB.00060-07 PMID: 17526700

34. Collins RF, Frye SA, Balasingham S, Ford RC, Tønjum T, Derrick JP (2005) Interaction with type IV pili induces structural changes in the bacterial outer membrane secretin PilQ. J Biol Chem 280: 18923–18930. doi: 10.1074/jbc.M411603200 PMID: 15753075

35. Campsall P, Laupland KB, Niven DJ (2013) Severe meningococcal infection: a review of epidemiology, diagnosis, and management. Crit Care Clin 29: 393–409. doi: 10.1016/j.ccc.2013.03.001 PMID: 23830646

36. Tobiason DM, Seifert HS (2006) The obligate human pathogen, Neisseria gonorrhoeae, is polyploid. PLoS Biol 4: 1069–1078. doi: 10.1371/journal.pbio.0040185 PMID: 16719561

37. Pagliarulo C, Salvatore P, De Vitis LR, Colicchio R, Monaco C, Tredici M, et al. (2004) Regulation and differential expression of gdhA encoding NADP-specific glutamate dehydrogenase in Neisseria menin-gitidis clinical isolates. Mol Microbiol 51: 1757–1772. doi: 10.1111/j.1365-2958.2003.03947.x PMID: 15009900

38. Bill NJ, Ii JAW (1977) Comparison of In Vitro Activity of Cephalexin, Cephradine, and Cefaclor. Mol Microbiol 11: 470–474.

39. Withers HL, Bernander R (1998) Characterization of dnaC2 and dnaC28 mutants by flow cytometry. J Bacteriol 180: 1624–1631. PMID: 9537356

40. Torheim NK, Boye E, Lùbner A (2000) The Escherichia coli SeqA protein destabilizes mutant DnaA204 protein. Mol Microbiol 37: 629–638. PMID: 10931356

41. Stokke C, Flåtten I, Skarstad K (2012) An easy-to-use simulation program demonstrates variations in bacterial cell cycle parameters depending on medium and temperature. PLoS One 7. doi: 10.1371/journal.pone.0030981 PMID: 22348034

42. National Center for Biotechnology Information (n.d.) Available: http://www.ncbi.nlm.nih.gov/protein/?term=RecG+Neisseria+meningitidis.

43. Stothard P (2000) The Sequence Manipulation Suite: JavaScript programs for analyzing and format-ting protein and DNA sequences. Biotech 281102–1104 28: 1102–1104.

44. Tamura K, Stecher G, Peterson D, Filipski A, Kumar S (2013) MEGA6: Molecular evolutionary genet-ics analysis version 6.0. Mol Biol Evol 30: 2725–2729. doi: 10.1093/molbev/mst197 PMID: 24132122

45. Rice P, Longden I, Bleasby A (2000) EMBOSS: the European Molecular Biology Open Software Suite. Trends Genet 16: 276–277. PMID: 10827456

46. Landau M, Mayrose I, Rosenberg Y, Glaser F, Martz E, Pupko T, et al. (2005) ConSurf 2005: The pro-jection of evolutionary conservation scores of residues on protein structures. Nucleic Acids Res 33: 299–302. doi: 10.1093/nar/gki370 PMID: 15980475

47. Kelly LA, Mezulis S, Yates C, Wass M, Sternberg M (2015) The Phyre2 web portal for protein model-ling, prediction, and analysis. Nat Protoc 10: 845–858. doi: 10.1038/nprot.2015-053 PMID: 25950237

48. Kanehisa M, Goto S, Sato Y, Kawashima M, Furumichi M, Tanabe M (2014) Data, information, knowl-edge and principle: back to metabolism in KEGG. Nucleic Acids Res 42: D199–D205. doi: 10.1093/nar/gkt1076 PMID: 24214961

49. Jerabek-Willemsen M, Wienken CJ, Braun D, Baaske P, Duhr S (2011) Molecular interaction studies using microscale thermophoresis. Assay Drug Dev Technol 9: 342–353. doi: 10.1089/adt.2011.0380 PMID: 21812660

50. Findlay WA, Redfield RJ (2009) Coevolution of DNA uptake sequences and bacterial proteomes. Genome Biol Evol 1: 45–55. doi: 10.1093/gbe/evp005 PMID: 20333176

51. Treangen TJ, Ambur OH, Tønjum T, Rocha EPC (2008) The impact of the neisserial DNA uptake sequences on genome evolution and stability. Genome Biol 9: R60. doi: 10.1186/gb-2008-9-3-r60 PMID: 18366792

52. Davidsen T, Rødland EA, Lagesen K, Seeberg E, Rognes T, Tønjum T (2004) Biased distribution of DNA uptake sequences towards genome maintenance genes. Nucleic Acids Res 32: 1050–1058. doi: 10.1093/nar/gkh255 PMID: 14960717

53. Goodman SD, Scocca JJ (1988) Identification and arrangement of the DNA sequence recognized in specific transformation of Neisseria gonorrhoeae. Proc Natl Acad Sci U S A 85: 6982–6986. PMID: 3137581

54. Bromberg Y, Rost B (2007) SNAP: predict effect of non-synonymous polymorphisms on function. Nucleic Acids Res 35: 3823–3835. doi: 10.1093/nar/gkm238 PMID: 17526529

55. Raghunathan S, Ricard CS, Lohman TM, Waksman G (1997) Crystal structure of the homo-tetrameric DNA binding domain of Escherichia coli single-stranded DNA-binding protein determined by multi-wavelength x-ray diffraction on the selenomethionyl protein at 2.9-A resolution. Proc Natl Acad Sci U S A 94: 6652–6657. doi: 10.1073/pnas.94.13.6652 PMID: 9192620

56. Buss JA, Kimura Y, Bianco PR (2008) RecG interacts directly with SSB: implications for stalled replica-tion fork regression. Nucleic Acids Res 36: 7029–7042. doi: 10.1093/nar/gkn795 PMID: 18986999

57. Yu C, Tan HY, Choi M, Stanenas AJ, Byrd AK, Raney KD, et al. (2016) SSB binds to the RecG and PriA helicases in vivo in the absence of DNA. Genes to Cells 21: 163–184. doi: 10.1111/gtc.12334 PMID: 26766785

58. McGlynn P, Lloyd RG (2002) Recombinational repair and restart of damaged replication forks. Nat Rev Mol Cell Biol 3: 859–870. doi: 10.1038/nrm951 PMID: 12415303

59. Thakur RS, Basavaraju S, Somyajit K, Jain A, Subramanya S, Muniyappa K, et al. (2013) Evidence for the role of Mycobacterium tuberculosis RecG helicase in DNA repair and recombination. FEBS J 280: 1841–1860. doi: 10.1111/febs.12208 PMID: 23438087

60. Robu ME, Inman RB, Cox MM (2004) Situational repair of replication forks: roles of RecG and RecA proteins. J Biol Chem 279: 10973–10981. doi: 10.1074/jbc.M312184200 PMID: 14701860

61. Azeroglu B, Mawer JSP, Cockram CA, White MA, Hasan AMM, Filatenkova M, et al. (2016) RecG Directs DNA Synthesis during Double-Strand Break Repair. PLoS Genet 12: 1–23. doi: 10.1371/journal.pgen.1005799 PMID: 26872352

62. Lloyd RG, Rudolph CJ (2016) 25 years on and no end in sight: a perspective on the role of RecG protein. Curr Genet. doi: 10.1007/s00294-016-0589-z PMID: 27038615

63. Abd Wahab S, Choi M, Bianco PR (2013) Characterization of the ATPase activity of RecG and RuvAB proteins on model fork structures reveals insight into stalled DNA replication fork repair. J Biol Chem 288: 26397–26409. doi: 10.1074/jbc.M113.500223 PMID: 23893472

64. Dennis PP, Bremer H (1974) Differential rate of ribosomal protein synthesis in Escherichia coli B/r. J Mol Biol 84: 407–422. doi: 10.1016/0022-2836(74)90449-5 PMID: 4618855

65. Diez A, Gustavsson N, Nyström T (2000) The universal stress protein A of Escherichia coli is required for resistance to DNA damaging agents and is regulated by a RecA/FtsK-dependent regulatory pathway. Mol Microbiol 36: 1494–1503. doi: 10.1046/j.1365-2958.2000.01979.x PMID: 10931298

66. Swanson J, Morrison S, Barrera O, Hill S (1990) Piliation changes in transformation-defective gonococci. J Exp Med 171: 2131–2139. PMID: 1972181

67. Wolfgang M, Lauer P, Park HS, Brossay L, Hebert J, Koomey M (1998) PilT mutations lead to simultaneous defects in competence for natural transformation and twitching motility in piliated Neisseria gonorrhoeae. Mol Microbiol 29: 321–330. PMID: 9701824

68. Tønjum T, Freitag NE, Namork E, Koomey M (1995) Identification and characterization of pilG, a highly conserved pilus-assembly gene in pathogenic Neisseria. Mol Microbiol 16: 451–464. doi: 10.1111/j.1365-2958.1995.tb02410.x PMID: 7565106

69. Helaine S, Carbonnelle E, Prouvensier L, Beretti JL, Nassif X, Pelicic V (2005) PilX, a pilus-associated protein essential for bacterial aggregation, is a key to pilus-facilitated attachment of Neisseria meningitidis to human cells. Mol Microbiol 55: 65–77. doi: 10.1111/j.1365-2958.2004.04372.x PMID: 15612917

70. Seib KL, Tseng H-JJ, McEwan AG, Apicella MA, Jennings MP (2004) Defenses against oxidative stress in Neisseria gonorrhoeae and Neisseria meningitidis: distinctive systems for different lifestyles. J Infect Dis 190: 136–147. doi: 10.1086/421299 PMID: 15195253

71. Bus JS, Gibson JE (1984) Paraquat: model for oxidant-initiated toxicity. Environ Health Perspect 55: 37–46. PMID: 6329674

72. Moore TDE, Hill C, Carolina N (1996) Interruption of the gpxA Gene Increases the Sensitivity of Neisseria meningitidis to Paraquat. J Bacteriol 178: 4301–4305. PMID: 8763962

73. Meddows TR, Savory AP, Grove JI, Moore T, Lloyd RG (2005) RecN protein and transcription factor DksA combine to promote faithful recombinational repair of DNA double-strand breaks. Mol Microbiol 57: 97–110. doi: 10.1111/j.1365-2958.2005.04677.x PMID: 15948952

74. Stohl EA, Seifert HS (2006) Neisseria gonorrhoeae DNA recombination and repair enzymes protect against oxidative damage caused by hydrogen peroxide. J Bacteriol 188: 7645–7651. doi: 10.1128/JB.00801-06 PMID: 16936020

75. Battistoni A (2003) Role of prokaryotic Cu,Zn superoxide dismutase in pathogenesis. Biochem Soc Trans 31: 1326–1329. doi:10.1042/. doi: 10.1042/ PMID: 14641055

76. Rudolph CJ, Upton AL, Lloyd RG (2009) Replication fork collisions cause pathological chromosomal amplification in cells lacking RecG DNA translocase. Mol Microbiol 74: 940–955. doi: 10.1111/j.1365-2958.2009.06909.x PMID: 19818016

77. Masai H, Tanaka T, Kohda D (2010) Stalled replication forks: making ends meet for recognition and stabilization. Bioessays 32: 687–697. doi: 10.1002/bies.200900196 PMID: 20658707

78. Meddows TR, Savory AP, Lloyd RG (2004) RecG helicase promotes DNA double-strand break repair. Mol Microbiol 52: 119–132. doi: 10.1111/j.1365-2958.2003.03970.x PMID: 15049815

79. Duncan T, Trewick SC, Koivisto P, Bates P, Lindahl T, Sedgwick B (2002) Reversal of DNA alkylation damage by two human dioxygenases. Proc Natl Acad Sci U S A 99: 16660–16665. doi: 10.1073/pnas. 262589799 PMID: 12486230

80. Nowosielska A, Smith SA, Engelward BP, Marinus MG (2006) Homologous recombination prevents methylation-induced toxicity in Escherichia coli. Nucleic Acids Res 34: 2258–2268. doi: 10.1093/nar/gkl222 PMID: 16670432

81. Campbell LEEA Yasbin RE (1979) Deoxyribonucleic acid repair capacities of Neisseria gonorrhoeae: absence of photoreactivation. J Bacteriol 140: 1109–1111. PMID: 118154

82. Carell T, Burgdorf LT, Kundu LM, Cichon M (2001) The mechanism of action of DNA photolyases. Curr Opin Chem Biol 5: 491–498. doi: 10.1016/S1367-5931(00)00239-8 PMID: 11578921

83. Essen LO, Klar T (2006) Light-driven DNA repair by photolyases. Cell Mol Life Sci 63: 1266–1277. doi: 10.1007/s00018-005-5447-y PMID: 16699813

84. Davidsen T, Tuven HK, Bjørås M, Rødland EA, Tønjum T (2007) Genetic interactions of DNA repair pathways in the pathogen Neisseria meningitidis. J Bacteriol 189: 5728–5737. doi: 10.1128/JB.00161-07 PMID: 17513474

85. Goosen N, Moolenaar GF (2001) Role of ATP hydrolysis by UvrA and UvrB during nucleotide excision repair. Res Microbiol 152: 401–409. doi: 10.1016/S0923-2508(01)01211-6 PMID: 11421287

86. Grossman L, Yeung AT (2007) The UvrABC endonuclease system of Escherichia coli. Mutat Res 1: 213–221.

87. Atkinson J, McGlynn P (2009) Replication fork reversal and the maintenance of genome stability. Nucleic Acids Res 37: 3475–3492. doi: 10.1093/nar/gkp244 PMID: 19406929

88. Marians KJ, Pasero P, Yeeles JTP (2016) Rescuing Stalled or Damaged Replication Forks.pdf: 1–16.

89. Sechman EV, Rohrer MS, Seifert HS (2005) A genetic screen identifies genes and sites involved in pilin antigenic variation in Neisseria gonorrhoeae. Mol Microbiol 57: 468–483. doi: 10.1111/j.1365-2958.2005.04657.x PMID: 15978078

90. Zegeye ED, Balasingham SV, Laerdahl JK, Homberset H, Kristiansen PE, Tønjum T (2014) Effects of conserved residues and naturally occurring mutations on Mycobacterium tuberculosis RecG helicase activity. Microbiology 160: 217–227. doi: 10.1099/mic.0.072140–0 PMID: 24169816